Adv Biochem Eng Biotechnol
DOI: 10.1007/10_2017_42


# Electron Transfer Between Enzymes and Electrodes

**Tanja Vidakovic-Koch**

**Abstract** Efficient electron transfer between redox enzymes and electrocatalytic surfaces plays a significant role in development of novel energy conversion devices as well as novel reactors for production of commodities and fine chemicals. Major application examples are related to enzymatic fuel cells and electroenzymatic reactors, as well as enzymatic biosensors. The two former applications are still at the level of proof-of-concept, partly due to the low efficiency and obstacles to electron transfer between enzymes and electrodes. This chapter discusses the theoretical backgrounds of enzyme/electrode interactions, including the main mechanisms of electron transfer, as well as thermodynamic and kinetic aspects. Additionally, the main electrochemical methods of study are described for selected examples. Finally, some recent advancements in the preparation of enzyme-modified electrodes as well as electrodes for soluble co-factor regeneration are reviewed.

T. Vidakovic-Koch (✉)
Max Planck Institute for Dynamics of Complex Technical Systems, Magdeburg, Germany
e-mail: vidakovic@mpi-magdeburg.mpg.de

## Graphical Abstract

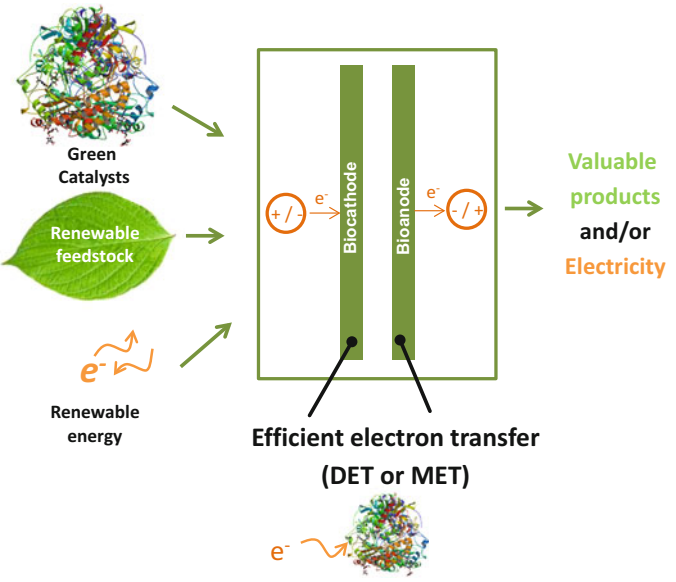


**Keywords** Direct electron transfer, Electrochemical co-factor regeneration, Electrochemical methods, Kinetics, Mediated electron transfer, Porous electrodes, Redox enzymes

## Contents

## 1 Types of Electron Transfer Mechanisms

The natural cycle of oxidoreductases involves several substrates. Normally, two substrates and two products are required, which corresponds to a so-called bi-bi reaction in the general nomenclature of enzyme reactions [1]. A convenient example of a bi-bi reaction is glucose oxidation by the glucose-oxidase enzyme, in accordance to:

$$\mathrm{D-glucose + O_2 \rightarrow D-glucono-1,5-lactone + H_2O_2} \quad (1)$$

Here, glucose and oxygen are the two substrates of this enzyme. The co-factor of glucose-oxidase is flavin adenine dinucleotide (FAD). FAD is usually deeply buried into the protein backbone, which normally excludes any direct electron transfer between FAD and the electrode. It is regenerated by its normal electron acceptor oxygen or artificial electron acceptors. Another enzyme that catalyzes glucose oxidation is nicotinamide adenine dinucleotide (NAD) dependent glucose 1-dehydrogenase:

$$\mathrm{D-glucose + NAD^+ \rightarrow D-glucono-1,5-lactone + NADH + H^+} \quad (2)$$

In this example, the two enzyme substrates are glucose and $NAD^+$ (or its phosphorylated derivate nicotinamide adenine dinucleotide phosphate [$NADP^+$]). $NAD^+$ is also the soluble enzyme co-factor, for which reason it is also the co-substrate. A similar case is NAD (NADP) dependent alcohol dehydrogenases, where alcohol is one substrate and $NAD^+$ or $NADP^+$ is the second one.

Some enzymes require more than two substrates. Examples of interest for electrobiotechnological applications are P450 monooxygenases. The most common reaction catalyzed by these enzymes is the insertion of molecular oxygen chemoselectively into the inert C-H bond of an organic substrate (RH), as follows:

$$\mathrm{RH + NADPH + H^+ + O_2 \rightarrow ROH + NADP^+ + H_2O} \quad (3)$$

Here, one of substrates (NADPH) is a common soluble co-factor of many enzymes.

During biotransformations (Eqs. 1, 2, and 3), oxidoreductases participate actively in the electron transfer between different substrates. The redox changes on the enzyme side take place mainly on co-factors. Some of the previously mentioned enzymes have only one co-factor (glucose oxidase, NAD dependent glucose 1-dehydrogenase), but many oxidoreductases have more than one. For example, cellobiose dehydrogenase has two co-factors (FAD and heme), whereas P450 often has three (FAD, flavin mononucleotide (FMN), and heme). If more co-factors are available, the electron transfer between enzyme substrates is accompanied by an interprotein electron transfer between co-factors. Usually, one of the co-factors is a catalytic center, whereas the other participates only in the electron transfer.

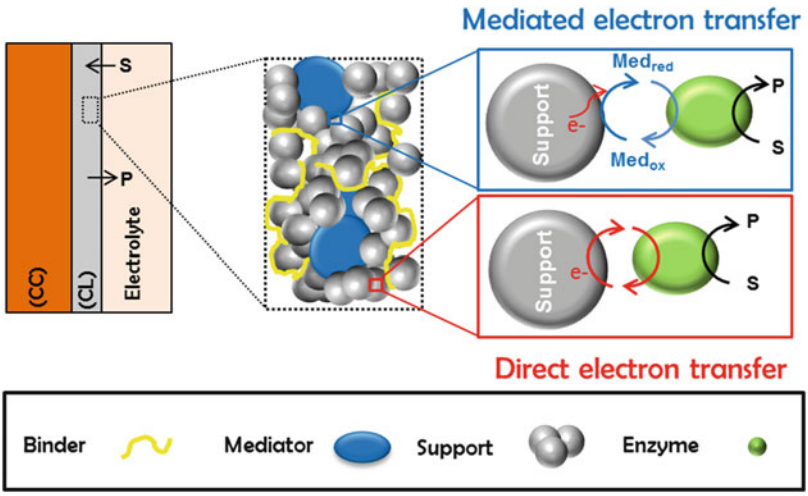


**Fig. 1** Schematic representation of a porous enzymatic electrode structure. Two mechanisms of enzyme/electron conductive support electron transfer are shown: mediated electron transfer (MET) and direct electron transfer (DET). *CC* current collector, *CL* catalyst layer, $Med_i$ i = ox, red (oxidized and reduced forms of a mediator), *S* substrate, *P* product. Reprinted from [2] with permission from Elsevier

In electrobiotechnology, one of the natural enzyme substrates is replaced by an artificial substrate (a so-called mediator) or an electrode itself. Alternatively, the natural enzyme substrates are regenerated electrochemically with the help of artificial substances or an electrode. The latter case applies if the natural enzyme substrate cannot be replaced (e.g. a co-substrate). The resulting electron transfer mechanisms are termed *mediated electron transfer* (MET) or *direct electron transfer* (DET). A schematic representation of a porous enzymatic electrode, showing its main components and the two main types of electron transfer mechanisms between enzymes and electron-conductive support, is shown in Fig. 1.

The different electron transfer mechanisms are further described in examples of glucose oxidase and NAD-dependent formate dehydrogenase. In a glucose-oxidase natural enzyme substrate, oxygen is replaced by an artificial substrate, which is then electrochemically regenerated. An advantage of using a substrate other than oxygen is the avoidance of $H_2O_2$ formation, which is one of the products in the natural cycle of glucose oxidase. As is well known, hydrogen peroxide can inhibit glucose-oxidase and influences its long-term stability. In the presence of a mediator, Eq. (1) can be rewritten as follows:

$$\mathrm{D-glucose} + \mathrm{Med_{ox}} \rightarrow \mathrm{D-glucono-1,5-lactone} + \mathrm{Med_{red}} \qquad (4)$$

In the next step, the mediator is regenerated electrochemically:

$$\mathrm{Med_{red}} \rightarrow \mathrm{Med_{ox}} + 2\mathrm{H^+} + 2\mathrm{e^-} \qquad (5)$$

where $\mathrm{Med_{ox}}$ and $\mathrm{Med_{red}}$ are the oxidized and reduced forms of the mediator.

The mediated regeneration of the NADH co-substrate on an example of formate dehydrogenase, can be represented as follows:

$$CO_2 + NADH + H^+ \rightarrow HCOOH + NAD^+ \quad (6)$$

$$NAD^+ + Med_{red} \rightarrow NADH + {Med_{ox}}^+ \quad (7)$$

$${Med_{ox}}^+ + H^+ + 2e^- \rightarrow Med_{red} \quad (8)$$

Alternatively to Eq. (7), $NAD^+$ can be directly reduced at the electrode surface, in which case a DET occurs:

$$NAD^+ + H^+ + 2e^- \rightarrow NADH \quad (9)$$

If NADH (NADPH) or its oxidized forms are enzyme substrates or co-substrates, its electrochemical regeneration or replacement by an artificial substrate is of high interest in electrobiotechnological applications. The main reasons for this are the high prices of these substrates, their difficult regeneration, and their tendency to decompose over time. The replacement of NADH (NADPH) is not straightforward because enzymes are optimized from nature for these electron donors. In some cases, protein engineering can tailor protein properties with respect to artificial substrates, as for example with P450 monooxygenase [3].

## *1.1 Some Mechanistic Aspects of Enzyme/Electrode Electron Transfer*

The scientific basis of electron transfer between an enzyme and an electrode surface is described by the Marcus theory [4]. The electron transfer rate between two species participating in a redox process depends on the driving force in terms of the Gibbs free energy change of the reaction (i.e. the potential difference), the distance between redox centers and the reorganization energy. If these conditions are favorable, then DET is possible, as reported in several cases. For example, different peroxidases show DET (cytochrome c peroxidase, horseradish peroxidase) [5, 6]. Laccase and bilirubin-oxidase are also able to exchange electrons directly with an electrode surface [7]. DET has also been reported for Ni-Fe hydrogenases [8]. This DET is favored because of the presence of iron-sulfur clusters, which act as an intraelectron transfer chain; they channel electrons from the Ni-Fe catalytic center to the protein surface, which reduces the distance between the catalytic center and the electrode surface. Furthermore, DET has been reported for bifunctional enzymes such as cellobiose dehydrogenase, where the heme co-factor can exchange electrons with the electrode [9].

The efficiency of DET depends strongly on the enzyme orientation on the surface. For example, oriented enzyme immobilization on the electrode surface, with the help of self-assembled monolayers (SAMs), results in more efficient electron transfer rates [4]. Other possibilities for oriented enzyme immobilization

were demonstrated by Zimmermann et al. [10], who reconstituted horseradish peroxidase (HRP) apo-enzyme on covalently attached heme co-factors on SAMs of a modified gold surface. However, this approach did not ultimately lead to improved electron transfer rates.

Although there is experimental evidence that isolated FAD can exchange electrons with an electrode [11], native enzymes with FAD cofactors (glucose-oxidase, cellobiose dehydrogenase) are normally not able to exchange electrons with the electrode surface. This is due to the isolated protein shell, which blocks electron transfer between the enzyme and electrode. FAD-dependent enzymes are able to perform DET only after partial removal of the protein shell by, for example, deglycosylation [12]. Yet, in number of cases, DET for GOx used in porous enzymatic electrodes with carbon nanotubes was reported. Some possible artefacts that lead to the conclusion of GOx DET were summarized elsewhere [13].

In free diffusive mediators, the electron transfer mechanism is similar to that of natural enzyme substrates. Namely, the mediator diffuses in and out of the enzyme, enabling the electron shuttle. If the mediator is immobilized, the mechanism of MET is not so clear. Some mechanistic interpretations of MET were discussed by Habermüller et al. [4], who emphasized the need for a degree of free diffusional movement of the redox mediator for efficient electron transfer. This can be achieved by a so-called electron-hopping mechanism, where the electron transfer distance between an enzyme co-factor and an electrode is reduced by dividing the overall electron transfer process into a sequence of electron-hopping reactions between adjacent redox mediator molecules. This approach might be used for redox relays in modified conducting polymers serving as an immobilization matrix. Some examples are modified polypyrrole matrices in ferrocene or osmium complexes. Additionally, some level of free diffusional movement of redox mediators can be achieved by the covalent attachment of the redox mediator via long and flexible spacer chains, either to the electrode surface, a suitable matrix, or the outer surface of the enzyme. The latter case uses the so-called whipping mechanism of MET.

## 2 Thermodynamics

Let us consider the following well-known reaction, which is catalyzed by the glucose-oxidase:

$$\mathrm{D-glucose} + \mathrm{O_2} \rightarrow \mathrm{H_2O_2} + \mathrm{D-glucono-1,5-lactone} \tag{10}$$

This biochemical redox reaction can be separated into two half-reactions, as follows:

$$\mathrm{D-glucono-1,5-lactone} + 2\mathrm{H^+} + 2\mathrm{e^-} \rightarrow \mathrm{D-glucose} \tag{11}$$

$$\mathrm{O_2} + 2\mathrm{H^+} + 2\mathrm{e^-} \rightarrow \mathrm{H_2O_2} \tag{12}$$

To satisfy the stoichiometry, the half-reactions (Eqs. 11 and 12) contain protons in addition to electrons. Normally, protons are excluded from biochemical reactions when the pH value (e.g. pH 7) is specified. Also following the electrochemical convention, both half-reactions are written as reduction reactions. The standard half-cell electrode potentials of Eqs. 11 and 12 can be calculated based on the thermodynamic data, with the hydrogen reaction as a reference half-cell reaction ($H_2$ gas activity and $H^+$ activity are assumed to be 1). The Gibbs free energy change can be calculated as follows:

$$\Delta_r G^o = \sum_{i=1}^{n} \nu_i \Delta_f G_i^o \tag{13}$$

Here, $\nu_i$ is a stoichiometric coefficient of the component $i$ in the biochemical reaction (e.g. Eqs. 11 and 12), having positive signs for the products of the reaction and negative for the reactants. The standard Gibbs free energies of formation ($\Delta_f G_i^o$) for selected biochemically relevant components are summarized in Table 1. Standard half-cell electrode potentials can be further calculated by applying the relationship between the standard electrode potential $E^o$ and the standard Gibbs free energy of the reaction. This can be derived from the first law of thermodynamics, assuming a reversible process at a constant temperature and pressure in which both mechanical work and electrical work are done [16], and assuming that the electrical work can be expressed as the work required to move charge $Q = nF$ by the potential difference $E$:

$$\Delta_r G^o = -nFE^o \tag{14}$$

Because biochemical reactions occur under conditions that are far away from standard conditions, electrode potentials at pH 7 instead of standard electrode

**Table 1** Standard Gibbs free energies of formation from the elements

| Substance | $\Delta_f G^o$/kJ mol$^{-1}$ | Reference |
|---|---|---|
| Acetaldehyde | −139.00[a] | [14] |
| $CO_2$ | −394.36 | [15] |
| D-glucono-1,5 lactone | −905.92[a] | [14] |
| D-glucose | −917.2 | [15] |
| Ethanol | −181.54[a] | [14, 15] |
| FAD | −79.83[a] | [14] |
| $FADH_2$ | −118.57[a] | [14] |
| Formaldehyde | −102.53 | [15] |
| $H_2O$ | −237.13 | [14] |
| $H_2O_2$ | −134.03 (−136.69) | [14, 15] |
| Methanol | −166.27 | [15] |
| $NAD^+$ | −39.89[a] | [14] |
| NADH | −17.24[a] | [14] |

[a]Calculated based on data in [14]

potentials are normally reported. Assuming a proton concentration of $10^{-7}$ and ideal solutions, electrode potentials at pH 7 ($E^{o,\#}$) can be recalculated from the values under standard conditions ($E^{o}$) using the Nernst equation:

$$E^{o,\#} = E^{o} + \nu_{H^+} \cdot 2.303 \frac{RT}{nF} \text{pH} \tag{15}$$

The values of half-cell electrode potentials at pH 7 are summarized in Table 2. The observed values in electroenzymatic systems are close to the calculated values in Table 2 only if the bioelectrochemical reaction is reversible and if it follows the DET mechanism. An example of such a reaction is the interconversion of $H^+$ and $H_2$ catalyzed by hydrogenase [17].

The data from Table 2 can be used for the calculation of reversible cell potentials, assuming standard concentrations of all involved species and standard conditions. Positive reversible cell potential values are characteristics of spontaneous systems, such as fuel cells (so-called galvanic systems); negative values are the characteristics of electrolytic systems (electrical energy has to be supplied to the cell in order to run the reaction in the desired direction). As can be seen in the example of methanol oxidation (Fig. 2), the oxidation reaction always takes place on the anode side and the reduction reaction on the cathode side, independent of the mode of operation (fuel cell or electrolyzer).

However, the charge (plus/minus) of the anode and cathode depends on the mode of operation: in electrolysis mode, the anode is more positive than the cathode; in the fuel cell operation, it is opposite. As it is clear from the discussion, reversible cell potentials are theoretical values, which are independent of the type of

**Table 2** Electrode potentials at pH 7 of selected biochemical reactions

| Half-reaction | $E^{o,\#}$ vs. SHE/V[a] | Reference |
|---|---|---|
| $CO_2 + 2H^+ + 2e^- =$ Formate | −0.524 | [b] |
| Gluconate- $+ 2e^- + 3H^+ =$ D-glucose $+ H_2O$ | −0.47 | [15] |
| $2H^+ + 2e^- = H_2$ | −0.414 | [15] |
| $6CO_2 + 24e^- + 24H^+ =$ D-glucose $+ 6H_2O$ | −0.404 | [b] |
| Formate $+ 3H^+ + 2e^- =$ Formaldehyde $+ H_2O$ | −0.400 | [b] |
| $CO_2 + 6H^+ + 6e^- =$ Methanol $+ H_20$ | −0.396 | [b] |
| D-glucono-1,5 lactone $+ 2H^+ + 2e^-$ = D-glucose | −0.356 | [b] |
| $NAD^+ + H^+ + 2e^- =$ NADH | −0.324 (−0.32) | [b][15] |
| Formaldehyde $+ 2H^+ + 2e^- =$ Methanol | −0.182 | [b] |
| FAD $+ 2H^+ + 2e^- = FADH_2$ | −0.213 (−0.2) | [b][15] |
| Acetaldehyde $+ 2H^+ + 2e^-$ = ethanol | −0.197 | [15] |
| $O_2$ (g) $+ 2H^+ + 2e^- = H_2O_2$ | 0.294 | [b] |
| $O_2$ (g) $+ 4H^+ + 4e^- = 2H_2O$ | 0.816 | [15] |
| $H_2O_2 + 2H^+ + 2e^- = 2H_2O$ | 1.335 | [b] |

[a]SHE, standard hydrogen electrode
[b]Calculated based on data in Table 1

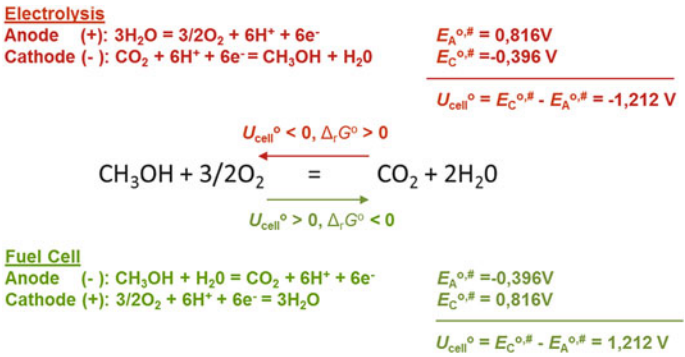


**Fig. 2** Half-cell reactions and electrode and reversible cell potentials for methanol to $CO_2$ conversion (and vice versa)

catalyst (metal or different enzymes). The values that are measured experimentally under open circuit conditions (no current flow through the cell) are denoted as open cell potential (ocp) values. The ocp values close to theoretical values were experimentally measured only for fast reversible reactions (e.g. hydrogen reaction) [17] or at high temperatures (which are not applicable for biotechnological systems).

Different mediators are used in combination with different cofactors (enzymes). An overview of some mediators used with FAD and NAD cofactors and their respective electrode potentials are provided in Table 3. The electrode potential values depend on the type of ions present in the solution, meaning that for most mediators only the formal potential values are reported.

## 3 Kinetics

### *3.1 Mechanisms of Bioelectrochemical Reactions*

Bioelectrochemical reactions comprise biochemical and electrochemical steps. Additionally, mass transfer of the involved soluble substances to and from the electrode surface has to be considered. Assuming that only substrates and products of a bioelectrochemical reaction are soluble, the mass transfer from the bulk to the electrode surface can be represented as follows:

$$\text{Substrate}_{\text{bulk}} \xrightarrow{\text{diff}} \text{Substrate} \tag{16}$$

$$\text{Product} \xrightarrow{\text{diff}} \text{Product}_{\text{bulk}} \tag{17}$$

Here, the substrate and product are any soluble enzyme substrate and product concentrations in the bulk and at the electrode surface.

**Table 3** Mediators typically used in connection with FAD and NAD cofactors and their respective formal redox potentials

| Mediator | Formal redox potential vs. SHE[a]/V | pH | Reference |
|---|---|---|---|
| *With FAD cofactor* | | | |
| 2-methyl-1-4-naphtoquinone on PLL | −0.07 | 7 | [18] |
| Os polymers | 0.01 (0.09) | 5 | [19, 20] |
| | 0.01 (0.04) | 7 | [19, 21] |
| Pyrroloquinoline quinone | 0.11 (0.08) | 7 (7.2) | [11, 22] |
| p-Benzoquinone | 0.6 | 7 | [23] |
| 8-hydroxyquinoline-5-sulfonic acid | 0.305 | 5 | [24] |
| Phenazine methosulfate | 0.32 | 6 | [25] |
| Tetrathiafulvalene | 0.419 | 7 | [26] |
| Poly(vinilferrocene) | 0.5 | 7 | [27] |
| Ferrocene monocarboxylic acid | 0.527 | 7 | [28] |
| *With NAD cofactor* | | | |
| Nile blue | −0.15 | 7 | [29] |
| Methylene green[b] | 0/0.15 | 6 | [30] |
| Poly(brilliant cresyl blue) | 0.09 | 7 | [31] |
| Poly(methylene blue) | 0.1 | 6 | [32] |

[a]$E$ vs. Ag/AgCl = $E$ vs. SHE-0.197 (V); $E$ vs. SCE = $E$ vs. SHE-0.24 (V)
[b]Methylene green shows two redox peaks

Biochemical steps are related to reactions between an enzyme and a substrate, while electrochemical steps are related to enzyme regeneration steps. Due to the variety of enzymes, different mechanisms of enzyme/substrate reactions are operative. In the following bi-bi mechanism, is shown in more detail because it is common to many oxidoreductases. A bi-bi reaction can be represented as follows:

$$\text{Substrate 1} + \text{Substrate 2} = \text{Product 1} + \text{Product 2} \tag{18}$$

This reaction holds for both the natural cycle of enzymes as well as for bioelectrochemical regeneration. The reaction (Eq. 18) commonly follows a double-displacement or Ping-Pong mechanism, where Substrate 1 binds first to the enzyme (Eq. 19). In this step, the enzyme is reduced/oxidized and Product 1 is formed. In the second step, the reduced/oxidized form of the enzyme binds Substrate 2 (Eq. 20). As a result, the enzyme is regenerated and Product 2 is formed. In electrobiotechnological applications, Substrate 2 is an artificial substrate (a mediator) or it is an electrode itself. Assuming MET, one can write the following:

$$E_{\text{red}} + \text{Substrate 1} \leftrightarrow E_{\text{ox}} + \text{Product 1} \tag{19}$$

$$E_{\text{ox}} + \text{Med}_{\text{ox}} \leftrightarrow E_{\text{red}} + \text{Med}_{\text{red}} \tag{20}$$

Here, $E_{\text{red}}$ and $E_{\text{ox}}$ are the reduced and oxidized forms of an enzyme.

The kinetics of biochemical (enzymatic) steps are commonly described by the Briggs–Haldane mechanism, which is a more generalized formulation of the Michaelis–Menten mechanism, including explicitly the rate constants of forward and backward reactions of enzyme substrate (ES) formation [33]. Assuming that the overall reaction is a reduction of Substrate 1 to Product 1, one can write the following:

$$\text{Substrate 1} + E_{\text{red}} \overleftrightarrow{k_1/k_{-1}} \text{ES} \tag{21}$$

$$\text{ES} \overleftrightarrow{k_{\text{cat}}} \text{Product 1} + E_{\text{ox}} \tag{22}$$

The kinetics of MET enzyme regeneration can be also described by the Briggs–Haldane mechanism:

$$E_{\text{ox}} + \text{Med}_{\text{red}} \overleftrightarrow{k_{m1}/k_{-m1}} \text{EM} \tag{23}$$

$$\text{EM} \overrightarrow{k_{m2}} \text{Med}_{\text{ox}} + E_{\text{ox}} \tag{24}$$

In most publications, the steps in Eqs. 23 and 24 are lumped together, showing only one effective rate constant ($k_{\text{m}}$), as follows:

$$E_{\text{ox}} + \text{Med}_{\text{red}} \overrightarrow{k_{\text{m}}} \text{Med}_{\text{ox}} + E_{\text{red}} \tag{25}$$

The electrochemical regeneration of the mediator can be represented as follows:

$$\text{Med}_{\text{ox}} + \text{ne}^- \overrightarrow{k_{\text{me}}} \text{Med}_{\text{red}} \tag{26}$$

In the simplest and most favorable case reaction (Eq. 26) involves transfer of only one electron.

In DET, instead of Eq. (25), one can write the following:

$$E_{\text{ox}} + \text{ne}^- \overleftrightarrow{k_{\text{e}}/k_{-\text{e}}} E_{\text{red}} \tag{27}$$

The reaction in Eq. 27 involves transfers of more than one electron, which are not likely to occur all at once; therefore, this step can be split into several one-electron steps. Assuming a two-electron process and the absence of intermediate chemical steps, one can write the following:

$$E_{\text{ox}} + \text{e}^- \overleftrightarrow{k_{\text{e1}}/k_{-\text{e1}}} \text{Int} \tag{28}$$

$$\text{Int} + \text{e}^- \overleftrightarrow{k_{\text{e2}}/k_{-\text{e2}}} E_{\text{red}} \tag{29}$$

## 3.2 Reaction Kinetics

The rate expressions for single steps in a DET or MET mechanism can be formulated based on the law of mass action, which assumes that the reaction rates are proportional to the activities (concentrations) of involved species. This approach is only valid for elementary steps in the mechanism. For lumped steps, empirical kinetic expressions can be also used. The rate expressions for the biochemical steps (Eqs. 21 and 22) can be formulated as follows:

$$r_1 = k_1\,\Gamma_{E_{\mathrm{red}}}(t)\,c_R(0,t) - k_{-1}\,\Gamma_{\mathrm{ES}}(t) \tag{30}$$

$$r_2 = k_2\,\Gamma_{\mathrm{ES}}(t) \tag{31}$$

Here, $k_i$ ($i = 1,-1,2$) are rate constants with units ($\mathrm{mol}^{-1}\ \mathrm{m}^3\ \mathrm{s}^{-1}$, $\mathrm{s}^{-1}$, $\mathrm{s}^{-1}$). $\Gamma_i$ ($i = E_{\mathrm{red}}$,ES) are surface concentrations of the reduced form of the enzyme and enzyme substrate complex with units ($\mathrm{mol\ m}^{-2}{}_{\mathrm{geo}}$).

For the DET mechanism, enzyme regeneration involves direct electron transfer between the enzyme and the electrode surface. The kinetics of steps (Eqs. 28 and 29) can be described by the empirical Butler-Volmer (BV) formulation or the more theoretical Marcus relationship (not discussed here). For the Butler-Volmer equation (Eq. 28), assuming an elementary step, one can write the following:

$$r_{\mathrm{DE\_1}} = \underbrace{k_{e10}\exp\left(-\frac{\alpha F}{\mathrm{RT}}\eta\right)}_{k_{e1}}\Gamma_{E_{\mathrm{ox}}}(t) - \underbrace{k_{-e10}\ \exp\left(\frac{\beta F}{\mathrm{RT}}\eta\right)}_{k_{-e1}}\Gamma_{\mathrm{Int}}(t) \tag{32}$$

Here, $\eta$ is defined as $\eta = E - E_{e1}^{o,\#}$, with $E$ being the electrode potential, $E_{e1}^{o,\#}$, standard electrode potential of the step (Eq. 28) at the studied pH, and $k_i$ ($i = \mathrm{e1},-\mathrm{e1}$) electrochemical rate constants with units $\mathrm{s}^{-1}$. In a similar manner, the rate of the second electrochemical step (Eq. 29) can be formulated. The DET kinetics can be simulated using the BV approach; however, the values of some parameters, such as transfer coefficients ($\alpha$,$\beta$), can deviate a lot from typical values in electrochemical kinetics. Transfer coefficient values of approximately 0.2 and below have been reported [6, 33].

The rate expression for the enzyme mediator step (Eq. 25), assuming an irreversible reaction and both enzyme and the mediator adsorbed at the surface, can be formulated as follows:

$$r_{\mathrm{EM}} = k_m\,\Gamma_{E_{\mathrm{ox}}}(t)\,\Gamma_{\mathrm{Med}_{\mathrm{red}}}(t) \tag{33}$$

The electrochemical rate of the mediator regeneration (Eq. 26) can be described by the BV equation.

In general, any of the biochemical or electrochemical steps in DET or MET mechanisms can be rate determining. For a DET mechanism with the steps in Eqs. 21, 22, 28 and 29, where electrochemical steps are considered to be

irreversible for the sake of simplicity, one can show that under steady-state conditions the reciprocal value of the overall reaction rate ($r_{\mathrm{DET\_SS}}$) is as follows:

$$\frac{1}{r_{\mathrm{DET\_SS}}} = \frac{1}{\Gamma_E}\left[\frac{1}{k_e} + \frac{c_R(0,SS) + K_M}{k_2 c_R(0,SS)}\right] \tag{34}$$

Here, $\Gamma_E$ is a total surface enzyme concentration (mol $\mathrm{m}^{-2}{}_{\mathrm{geo}}$), and $k_e$ and $K_M$ are overall constants of electrochemical (Eqs. 28 and 29) and biochemical (Michaelis-Menten constant) (Eqs. 21 and 22) steps, defined as follows:

$$k_{\mathrm{e}} = \frac{k_{\mathrm{e1}} k_{\mathrm{e2}}}{k_{\mathrm{e1}} + k_{\mathrm{e2}}} \tag{35}$$

$$K_M = \frac{k_{-1} + k_2}{k_1} \tag{36}$$

Equation 34 demonstrates the series connection between the "resistances" of the electrochemical and biochemical steps. The overall control of the reaction is influenced by the overpotential, showing in general electrochemical control at lower overpotentials and biochemical at higher overpotentials. Because the second term in Eq. 34 contains the reactant concentration, the possibility of a mass transfer limitation at higher overpotentials is given. If biochemical and mass transfer resistances are of the same order of magnitude, mixed-control conditions can be observed experimentally. This is nicely demonstrated in the example of a hydrogen reaction catalyzed by *Desulfovibrio vulgaris Miyazaki F* (*DvMF*) [NiFe]-hydrogenase (Fig. 3). This reaction shows very fast kinetics, which quickly reach limiting current conditions. The limiting currents are more dependent on the concentration than the rotation rate, indicating predominant biochemical reaction control. In the direction of hydrogen evolution, no dependence on the rotation rate is observed. The small influence of the hydrogen concentration is probably caused by the reversibility of the hydrogen reaction.

Based on Faraday's law, in electrochemical systems, the reaction rate is proportional to the measured current. The same proportionality holds for the rate of the bioelectrochemical reaction and the measured current. For DET, the steady-state current density value is proportional to the steady-state reaction rate (Eq. 34) as follows:

$$j_{\mathrm{DET\_SS}} = nFr_{\mathrm{DET\_SS}} \tag{37}$$

Here, $n$ is the number of exchanged electrons (in the present example, $n = 2$).

## 3.3 Balance Equations

The overall reaction rate (Eq. 34) is concentration dependent. To get the concentration profile of the reactant (product) mass, the balance equation has to be solved.

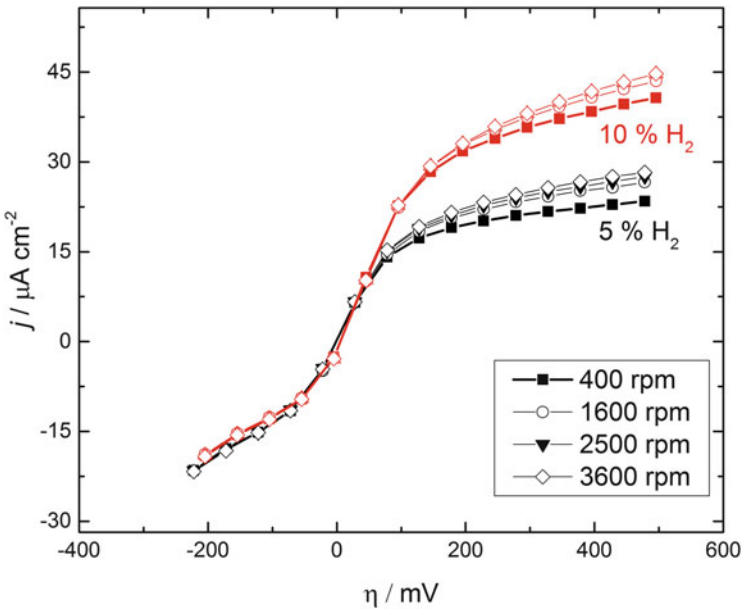


**Fig. 3** Influence of the rotation rate on steady-state polarization curves for a hydrogen reaction catalyzed by *DvMF* [NiFe]-hydrogenase at pH 7 and two different $H_2$ concentrations (reference electrode: SCE, temperature 20°C, electrode surface area 0.0314 $cm^2$). Unpublished results, courtesy of Dr. Olaf Rüdiger, Max Planck Institute for Chemical Energy Conversion

Assuming an electroenzymatic reaction at the flat electrode surface (Fig. 4a), it reads:

$$\frac{\partial c_\alpha(z,t)}{\partial t} = -\frac{\partial\left(g_{k,\alpha} + c_\alpha v_k\right)}{\partial z_k} \tag{38}$$

where $g_{k,\alpha}$ is a diffusion flux of the component α (mol $m^{-2}{}_{geo}$ $s^{-1}$), $v_k$ is the average molar velocity (m $s^{-1}$), and $z_k$ ($k = 1,2,3$) is the space coordinates. Assuming the concentration changes only in one $z_k$ direction, with a constant value of $v_k$ velocity and validity of Fick's law, one obtains the following:

$$\frac{\partial c_\alpha(z,t)}{\partial t} = D_{\alpha,H_2O}\frac{\partial^2 c_\alpha(z,t)}{\partial z^2} - v\frac{\partial c_\alpha(z,t)}{\partial z} \tag{39}$$

Here, 5 $D_{\alpha,H_2O}$ is a binary diffusion coefficient of component $\alpha$ in water. Equation 39 is applicable for the description of concentration profiles of components reacting on a rotating disc electrode (RDE). This equation can be further simplified by neglecting the convective contribution (the last term in Eq. 39) to the concentration change. This is usually the case in the thin layer close to the electrode surface—the

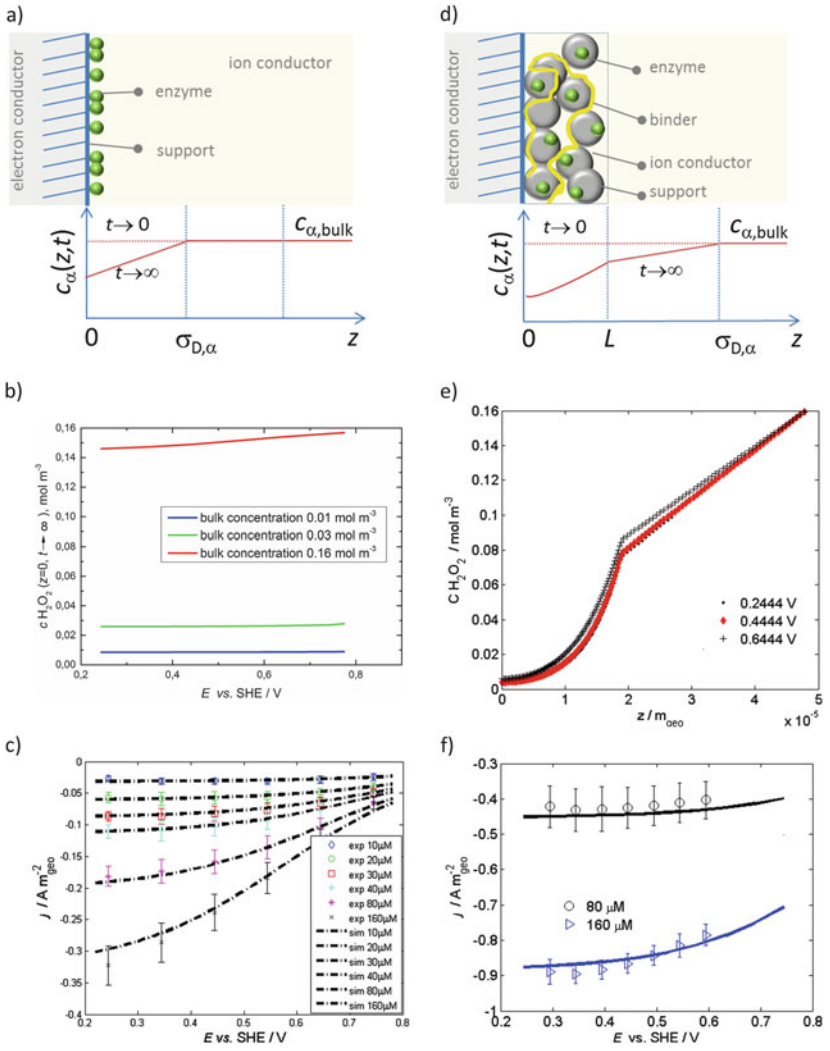


**Fig. 4** (**a**) Schematic representation of a thin-film enzymatic electrode with (**b**) steady-state surface concentration of $H_2O_2$ and (**c**) geometrical current densities (calculated based on [33]) and (**d**) schematic representation of a porous enzymatic electrode with (**e**) steady-state $H_2O_2$ concentration profiles along the porous catalyst layer and (**f**) geometrical current density. Parts **e** and **f** are reprinted from [5] with permission from Elsevier

so-called Nernstian diffusion layer—where the velocity falls below 1% of its maximal value in the bulk and mass transport is mainly dependent on diffusion [34]. (A schematic representation of concentration profiles at time zero and infinitely long time are shown in Fig. 4a.)

To solve this equation, the initial and boundary conditions are required. For RDE, they are as follows:

$$z = 0 \; D_{\alpha,H_2O} \frac{\partial c_\alpha(z,t)}{\partial z} | z = 0 = \sum_{m=1}^{R} \nu_{\alpha m} r_m(t) \tag{40}$$

$$z = \delta_{D,\alpha} \; c_\alpha(\delta_{D,\alpha}, t) = c_{\alpha,\infty} \tag{41}$$

Here, $R$ is the number of reaction steps where the component $\alpha$ is involved, $\nu_{\alpha m}$ is the stoichiometric coefficient of component $\alpha$ in the respective step, $r_m(t)$ is the rate of the surface reaction (e.g., Eq. 30), and $\delta_{D,\alpha}$ is the thickness of the diffusion layer of component $\alpha$, defined as follows:

$$\delta_{D,\alpha} = 1.61 (D_{\alpha,H_2O})^{1/3} \nu^{1/6} w^{-1/2} \tag{42}$$

where, $\nu$ is the kinematic viscosity of the solution and $\omega$ is the electrode rotation rate. The solution of Eq. 39 gives a concentration profile over time and space coordinates. The calculated steady-state values of the substrate surface concentrations ($c_{\text{Substrate}}(0,t)$) as a function of applied electrode potential for three different bulk concentrations are shown in Fig. 4b. The surface concentrations deviate a bit from bulk concentrations, indicating the small influence of mass transport conditions. The presented profiles are calculated based on the model presented in [33], which describes the kinetics of hydrogen peroxide reduction by horseradish peroxidase on a flat enzyme-modified RDE. The experimental and calculated steady-state polarization curves [33] are shown in Fig. 4c.

Most technical systems use porous electroenzymatic electrodes (Fig. 4d). In such cases, Eqs. 38 and 39 are valid for the mass transfer description in the solution. Depending on conditions, one can also expect concentration changes inside of the enzymatic electrode, in which case the following mass balance equation can be formulated [5, 35]:

$$\varepsilon \frac{\partial c_\alpha(z,t)}{\partial t} = D^{\text{eff}}_{\alpha,H_2O} \frac{\partial^2 c_\alpha(z,t)}{\partial z^2} + a \sum_{m=1}^{R} \nu_{\alpha m} r_m \tag{43}$$

Here, $\varepsilon$ is the volume fraction of the liquid phase inside of the enzymatic electrode porous structure ($m^3_{\text{L}}/m^3_{\text{geo}}$), $D^{\text{eff}}_{\alpha,H_2O}$, effective diffusivity and "$a$" ($m^2_{\text{act}}/m^3_{\text{geom}}$) is the internal surface of the electroenzymatic electrode where the reactions ($r_m$) take place per its geometrical volume. The calculated concentration profiles of $H_2O_2$ in a porous electroenzymatic electrode are shown in Fig. 4e [5]. The linear decrease of the concentration in the diffusion layer and the exponential decrease in the catalyst layer (CL) can be observed. The profiles are almost independent of potential; strong reactant depletion in the CL is seen at all potentials.

For dynamic operation, in addition to mass balance, a charge balance equation has to be defined [5, 36]:

$$c_{\mathrm{DL}} \frac{\partial E(z,t)}{\partial t} = -\imath(z,t) + aF \sum_{m=1}^{R} n_m r_m \tag{44}$$

where, $c_{\mathrm{DL}}$ is double layer capacity F $\mathrm{m}^{-2}{}_{\mathrm{act,}}$ $\imath$ is the local current density (A $\mathrm{m}^{-2}{}_{\mathrm{act}}$), and $n_{\mathrm{m}}$ is the number of exchanged electrons in the reaction step $m$. In a DET mechanism, the steps in Eqs. 28 and 29 will contribute electrons, while in the MET case step (Eq. 26) will contribute electrons. The electrode potential value ($E(z,t)$) is defined as follows:

$$E(z,t) = \phi_E^{\mathrm{CL}}(z,t) - \phi_I^{\mathrm{CL}}(z,t) \tag{45}$$

Here, $\phi_E^{\mathrm{CL}}(z,t), \phi_I^{\mathrm{CL}}(z,t)$ are potential field profiles in the electron and ion conducting phases respectively; the superscript CL refers to the catalyst layer. The potential profiles in electron and ion conducting phases follow from:

$$0 = \frac{\partial}{\partial z}\left(\gamma_E^{\mathrm{CL}} \frac{\partial \phi_E^{\mathrm{CL}}(z,t)}{\partial z}\right) - a\imath(z,t) \tag{46}$$

$$0 = \frac{\partial}{\partial z}\left(\gamma_I^{\mathrm{CL}} \frac{\partial \phi_I^{\mathrm{CL}}(z,t)}{\partial z}\right) - a\imath(z,t) \tag{47}$$

Alternatively, it can be assumed that there is no potential distribution throughout the catalyst layer. In this case, the electrode potential, $E$(t), is only a function of time and is equal to the applied potential corrected for ohmic drop resistance.

$$E(t) = E_{\mathrm{apl}}(t) - R_\Omega\, j(t) \tag{48}$$

Here, $j$ is the global current density value (A $\mathrm{m}^{-2}{}_{\mathrm{geo}}$) and $R_\Omega$ ($\Omega$ $\mathrm{m}^{2}{}_{\mathrm{geo}}$) is the electrolyte resistance. The global current density (experimentally measurable) can be obtained by integration of the local current values over the electrode thickness (in a one-dimensional system) according to the following [5, 36]:

$$j(t) = \int_0^L a\imath(z,t)\mathrm{d}z \tag{49}$$

where, $L$ is the electrode thickness. The calculated and experimental current densities for the same example of a porous HRP electrode are shown in Fig. 4f [5].

## 4 Methods of Study

Electrochemical methods are very convenient to study electron transfer between enzymes and electrodes. The main advantage of these methods over other methods of measurements (e.g. spectroscopic) is the possibility of direct measurement of the reaction rate in the form of electrical current (Eqs. 37 or 49). In this section, some

basic electrochemical methods of measurement are demonstrated using selected examples with relevance to electrobiotechnological applications. For further reading, please consider [37, 38].

In general, an electrochemical cell and a device (normally a potentiostat/galvanostat) that can monitor, apply, or control the potential or current input/output variables of an electroenzymatic system are needed to perform an electrochemical measurement. There are two types of electrochemical cells: two- and three-electrode setups. Two-electrode cells are used in technical applications, whereas three-electrode setups are mainly used for research purposes. In the two-electrode cell, one electrode is the anode and the second electrode is the cathode. On the anode side, an oxidation reaction takes place, whereas reduction occurs on the cathode. The cell potential is always expressed as the difference between cathode and anode potentials. In a three-electrode setup, the electrodes are termed the working (WE), counter (CE), and reference electrodes (RE). The electrochemical reaction takes place on the WE, which is the subject of the study. This electrochemical reaction can be either oxidation or reduction, while the complementary reaction will take place on the CE. The third electrode, the RE, is used to monitor or set the potential of the WE. The potential difference between the WE and the RE is the electrode potential. Common reference electrodes are the saturated calomel electrode (SCE) and the silver/silver chloride electrode (Ag/AgCl). In the two-electrode setup, the current is measured between the cathode and anode; in the three-electrode setup, it is measured between the WE and CE (in both cases, they are termed cell currents).

Electrode/cell potentials and cell currents can be set and measured with a potentiostat or galvanostat, which are fundamental tools in electrochemistry. A potentiostat or galvanostat can operate in a potentiostatic/voltastatic or galvanostatic mode of operation. In the potentiostatic mode, the potential difference between the WE and RE (electrode potential) is set, while the cell current is measured. In the voltastatic mode, the cell potential (the potential difference between the cathode and anode) is set, while the cell current is measured (Fig. 5a). During galvanostatic operations, the cell current is set, while electrode potential ($E_{WE\_RE}$) or cell potential ($U_{C\_A}$) for three- and two-electrode setups, respectively, are measured. The schematic representations of two- and three-electrode setups and control and measured variables for voltastatic/potentiostatic modi of operation are shown in Fig. 5.

As can be seen in Fig. 5b, the $E_{WE\_RE}$ includes the ohmic drop in the solution between the tip of a so-called Luggin capillary and the WE electrode ($j_{cell}R_{\Omega}$). Some devices are able to compensate for the ohmic drop online with the help of positive feedback or a current-interrupt technique. This is especially important if significant currents flow through the cell at significant ohmic resistances. In electrobiotechnological applications, currents are usually low, but the ohmic resistances can be quite large because neutral and close-to-neutral solutions have lower conductivity due to low proton concentrations compared to strong acidic or alkaline solutions. It can be calculated that a 0.1 M phosphate buffer at pH 5 has an ohmic resistance of approximately 3 m$\Omega$ m$^2$ [33].

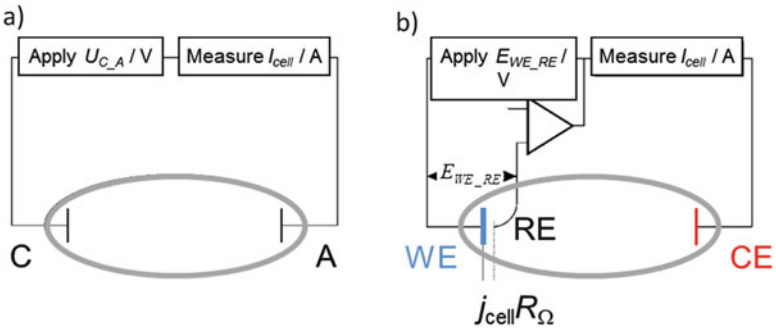


**Fig. 5** Schematic representation of (**a**) two- and (**b**) three-electrode setups showing the control and measured variables in (**a**) voltastatic and (**b**) potentiostatic modi of operations

Compared to nonelectrical variables, current and electrode/cell potentials can be more easily modulated. Therefore, there is a broad range of electrochemical methods where electrical input variables are varied in a form of step, linear, or sinusoidal signals. The most common are stationary polarization, cyclic/linear sweep voltammetry, and electrochemical impedance spectroscopy.

## *4.1 Stationary Polarization*

In stationary polarization, a step change of potential or current is applied as an input, while a transient change of the current or potential is recorded as an output. A record of current change over time is termed chronoamperometry, while a record of the potential change over time is termed chronopotentiometry. Figure 6 shows experimental data obtained by using a porous enzymatic electrode employing HRP as a WE in a three-electrode set-up in a potentiostatic mode of operation ($E_{\mathrm{WE\_RE}}$ is set, while $I_{\mathrm{cell}}$ is measured). As can be seen, the current response contains both transient and steady-state parts. Although the transient part of the response can yield valuable information about the system, in stationary polarization only the steady-state part of the response is evaluated. By plotting steady-state potential versus steady-state current values, one can obtain a so-called polarization curve. These data are shown in Fig. 6b. The current points (Fig. 6b) measured after 60 and 120 s do not show significant differences, indicating steady-state conditions.

Stationary polarization is also used for the characterization of electroenzymatic fuel cells or electrolyzers. In this case, the potential difference between cathode and anode ($U_{\mathrm{C\text{-}A}}$, cell potential) is set and the cell current is measured over time. It is common to present this data in the form of a cell potential versus cell current plot (Fig. 7a) (x-y axes are switched compared to a three-electrode set-up). The electrochemical behavior of three different electroenzymatic reactors operating under the same conditions (temperature, glucose concentration, flow rates) can be

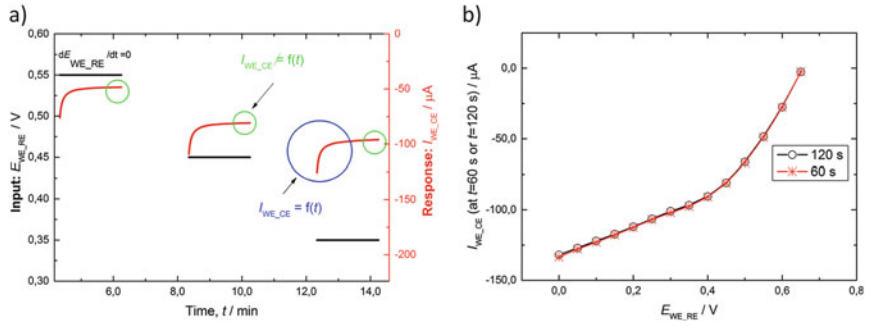


**Fig. 6** Potentiostatic stationary polarization measurements on an example three-electrode setup. (**a**) Change of the input and response variables over time and (**b**) polarization curves. WE: HRP modified porous enzymatic electrode, CE: platinum wire, RE: SCE. Room temperature, 0.1 M phosphate buffer, pH = 6. Adapted from [39]

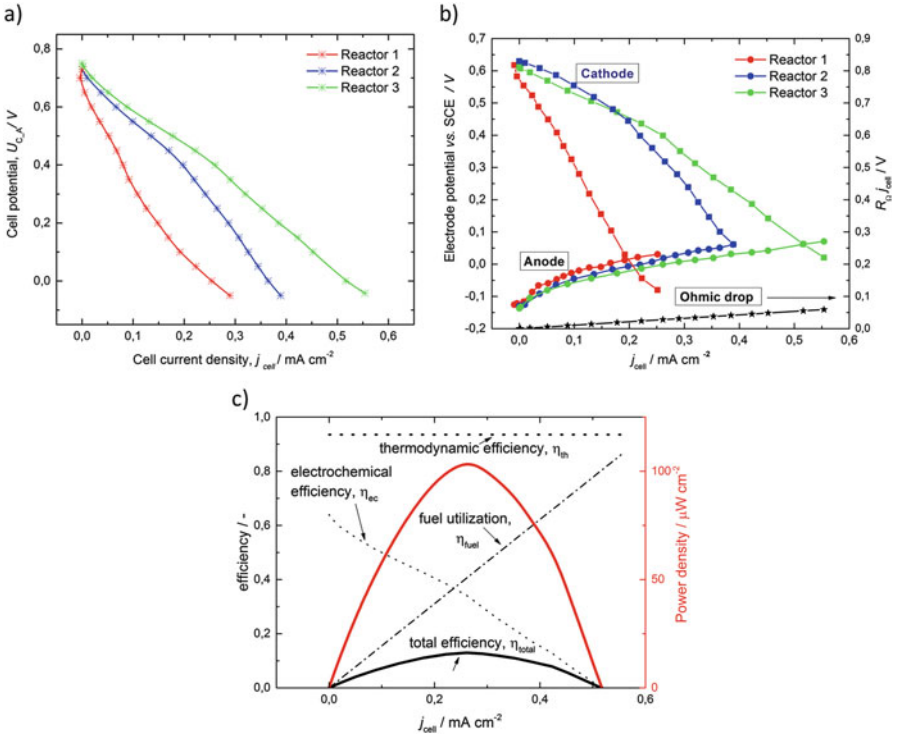


**Fig. 7** Potentiostatic stationary polarization measurements on an example of an enzymatic fuel cell (two-electrode set-up): (**a**) polarization curves, (**b**) electrode potentials and ohmic drop in an electrolyte, and (**c**) power density and efficiency curves. C: GOx-HRP porous enzymatic electrode, A: GOx/TTF porous enzymatic electrode, RE: SCE. Room temperature, 0.1 M phosphate buffer, pH = 6, flow rate 10 mL min$^{-1}$; (**a**) is reprinted from [40, 41]

visualized in Fig. 7a. From these data, it is difficult to rationalize why the performance of Reactor 3 is better than of Reactor 1. The fuel cell or electrolyzer cell potential current characteristics can be described with the following equation:

$$U_{\text{cell}} = E_c - E_A - \sum jR_i = \left(E_C^{o,\#} + \eta_C\right) - \left(E_A^{0,\#} + \eta_A\right) - \sum jR_i \tag{50}$$

Equation (50) shows clearly that the overall performance is influenced by losses on the cathode and anode sides as well as ohmic losses. Providing that an RE can be inserted into a fuel cell or electrolyzer, it becomes possible to measure anode and cathode potentials during a fuel cell's or electrolyzer's operation. Depending on the position of the RE, the measured values will contain contributions of the ohmic resistance of the electrolyte between the electrodes. This contribution can be estimated based on the value of electrolyte resistance ($R_\Omega$) obtained either by calculations or measurements (e.g. from electrochemical impedance spectroscopy [EIS]; see below). The potentials of single electrodes as well as ohmic resistance under fuel cell conditions are shown in Fig. 7b.

Compared to Fig. 7a, b offers some additional information. It follows that the contribution of the ohmic resistances in the electrolyte to observed losses is low. It is also clear that the cathode contributes more to potential losses than the anode (~600 mV on the cathode side compared to ~200 mV on the anode side are needed to achieve max current densities). The cathode in Reactor 3 can reach higher current densities than in the other two reactors, indicating a higher number of electrochemically active enzymes. The overall electrochemical performance is influenced by the enzymatic cathode.

For fuel cell operation, it is also important to know which power density ($P = U_{\text{C\_A}} \times I_{\text{cell}}/A_{\text{geo}}$) can be provided by the fuel cell. This information can be obtained from polarization curves by plotting $P$ versus the cell current density ($j_{\text{cell}} = I_{\text{cell}}/A_{\text{geo}}$) (Fig. 7c). The power density current curve shows a characteristic maximum, which corresponds to the maximal efficiency of the fuel cell (Fig. 7c). The total fuel cell efficiency can be easily calculated as follows:

$$\eta_{\text{total}} = \underbrace{\frac{\Delta_r G^o}{\Delta_r H^o}}_{\eta_{\text{th}}} \cdot \underbrace{\frac{U_{\text{cell}} nF}{\Delta_r G^o}}_{\eta_{\text{ec}}} \cdot \underbrace{\frac{j_{\text{cell}} A_{\text{geo}}}{nF G_{G,\text{in}}^A}}_{\eta_{\text{fuel}}} \tag{51}$$

where $G_{G,\text{in}}^A$ is flow rate of the glucose solution at the inlet, $\eta_{\text{th}}$ is thermodynamic efficiency, $\eta_{\text{ec}}$ is electrochemical efficiency, and $\eta_{\text{fuel}}$ is fuel utilization efficiency. The total efficiency in Fig. 7c is calculated by assuming a fuel cell surface area of 1 $m^2$. Smaller surface areas will result in lower efficiency (~0.001% for 1 $cm^2$ of surface area). As can be seen in Fig. 7c, the electrochemical efficiency is decreasing with an increase of the current density, while at the same time the fuel utilization is increasing. The tradeoff between these two trends determines the overall efficiency.

## 4.2 Cyclic Voltammetry

In cyclic voltammetry (CV), cell potential ($U_{C\text{-}A}$) or electrode potential ($E_{WE\text{-}RE}$) as an input is changed between the starting and maximum levels at a constant sweep rate (Fig. 8a) and cell current is recorded as a response (Fig. 8b). The common sweep rate values are between $10^{-3}$ and $10^{3}$ V $s^{-1}$. The cycle shown in Fig. 8a can be repeated $n$ times; usually, the potential is cycled until the current stops changing. CV is more often used for characterization of WE in a three-electrode setup, but it can be used also for two-electrode setup characterizations. In a three-electrode setup, the potential difference $E_{WE\text{-}RE}$ is set. This potential difference also contains the contribution of the ohmic drop in the electrolyte. Because the electrochemical reaction is driven only by the ohmic drop's free potential difference, it is important to correct the ohmic drop's contribution during a CV experiment. The reason can be easily seen in Fig. 8a. The red line shows the time change of the ohmic drop's corrected $E_{WE\_RE}$ potential, which is calculated assuming an electrolyte resistance of 3 mΩ $m^2$; deviations from the expected linear change of the potential can be observed, $dE_{WE\_RE}/dt$ is no longer constant, which is a main assumption of CV measurements. The data in a CV experiment are normally presented in the form of current-potential characteristics, which is called cyclic voltammogram (Fig. 8c). The yellow rectangle in Fig. 8c corresponds to the behavior of a so-called ideally polarizable electrode showing only double-layer charging (no Faradaic reaction). The measured current then corresponds to pure capacitive current, where in this case holds as follows:

$$I_{WE-CE} = I_{capacitive} = c_{DL} \cdot v \, A_{geo} \tag{52}$$

with $v$ being the sweep rate (V $s^{-1}$). The behavior of a real porous enzymatic electrode shows some deviations compared to the ideally polarizable electrode, especially at more positive and more negative potentials. In the potential region from approximately 0.2 to 0.4 V, the behavior corresponds almost to the expected behavior of a pure capacitor and can be used for the estimation of double-layer capacitance.

Cyclic voltammetry experiments are fast and simple to perform. They provide good orientation on system properties, such as the potential region where the reaction takes place, and they provide an orientation on rate-determining steps. Additionally, CV can be also used for estimation of the enzyme surface coverage (enzyme total surface concentration). The surface coverage of most DET enzymes at electrode surfaces is very low, for which reason redox peaks showing direct electron exchange between an enzyme and an electrode cannot always be observed. To exemplify the surface coverage determination, determination of covalently adsorbed PQQ mediator coverage on a cysteamine-modified gold electrode is chosen (Fig. 8d) [42]. The well-defined redox peaks can be observed in Fig. 8d. The areas under these peaks are integrated using the straight lines as a background. The values of 2.42 and 2.48 μA V were estimated for the anodic and cathodic peaks,

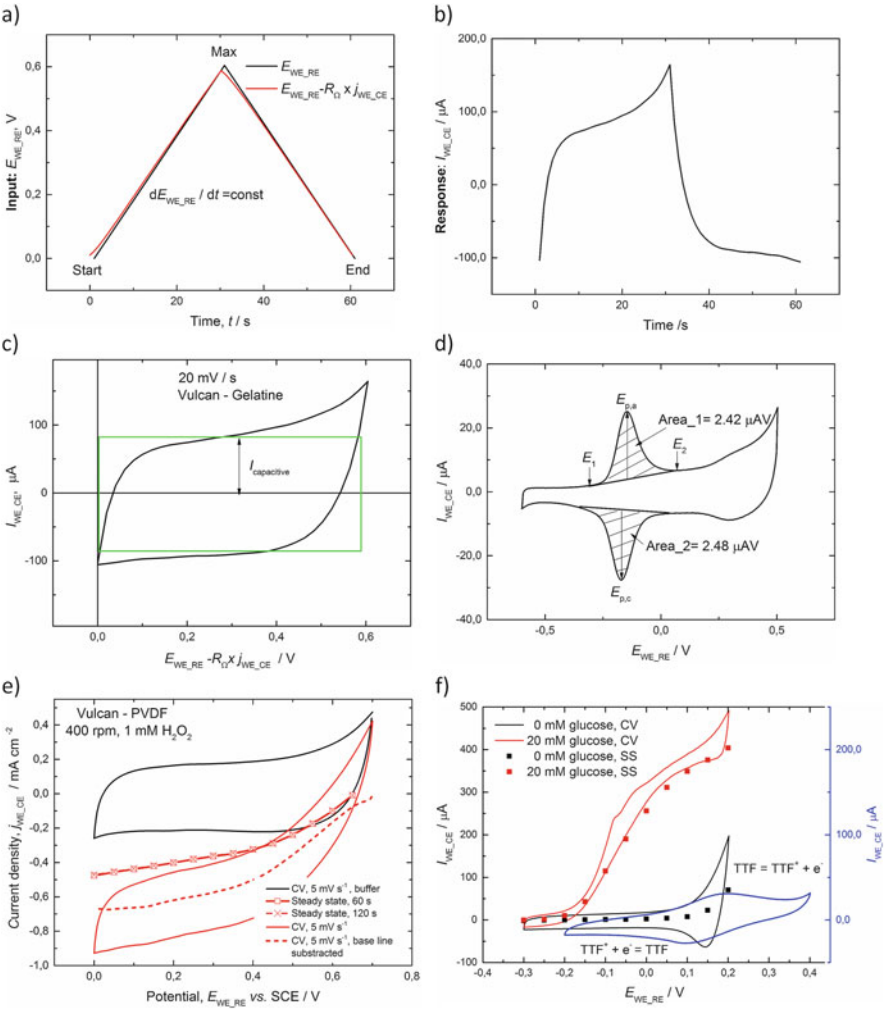


**Fig. 8** Cyclic voltammetry measurements on an example of a three-electrode setup. (**a**) Input $E_{WE\_RE}$ potential change over time. (**b**) Response cell current change over time. (**c**) Cyclic voltammetry of a porous HRP enzymatic electrode without Faradaic reaction, 20 mV s$^{-1}$. (**d**) Cyclic voltammogram of an electrode showing a Faradaic reaction related to the surface adsorbed species (PQQ modified Au electrode at pH 7.2, 20 mV s$^{-1}$). (**e**) Comparison between stationary polarization and CV in a DET mechanism at pH 6 and room temperature. (**f**) Comparison between stationary polarization and CV (5 mV s$^{-1}$) in a MET mechanism. The blue line corresponds to CV (5 mV s$^{-1}$) of a tetrathiafulvalene (TTF) dispersed in Nafion film modified graphite electrode, pH = 7.2, 37°C. Further conditions: 0.1 M phosphate buffer. (**d**) is reprinted from [42] with permission from the author, (**e**) is reprinted from [39]. (**f**) is reprinted from [43] with permission from Elsevier

respectively. These areas are divided by sweep rate, number of exchanged electrons, electrode geometric surface area, and the Faraday constant. The PQQ coverage of $1.33 \times 10^{-9}$ mol cm$^{-2}{}_{geo}$ and $1.37 \times 10^{-9}$ mol cm$^{-2}{}_{geo}$ is calculated. The roughness of the gold electrode is estimated to be approximately 25.

If the reactant is added to the reaction mixture, the Faradaic current will add up to the capacitive current. Subtraction of the capacitive currents measured without the reactant in the reaction mixture from the total current in presence of reactant will roughly result in the Faradaic current of the reaction. Although the capacitive current is dependent on the sweep rate, the activation current should be independent. This holds only if there is no mass transfer limitation in the system. If the latter is the case, the Faradaic current will also depend on the sweep rate because the concentration profiles throughout the catalyst layers will require some time to establish. Therefore, the currents obtained by subtraction of the capacitive contribution will still be sweep rate dependent; in the limiting case of very slow sweep rates, they will approximate the steady-state currents. This is demonstrated in Fig. 8d, where the currents obtained by the subtraction of CV currents and steady-state responses are compared. The same can be followed in an example of MET (Fig. 8f). Tetrathiafulvalene (TTF) was used as a mediator, which starts to "dissolve" in the absence of glucose at more positive potentials (black curve in Fig. 8f). If the direction of the potential is reversed, a small reduction peak can be observed. This behavior can be attributed to the solubility of $TTF^+$ formed in an aqueous solution. If the TTF is captured close to the surface, such as in a Nafion polymer (blue line), almost symmetrical oxidation/reduction peaks can be observed (Fig. 8f, blue line).

One of disadvantages of CV is the need for a complicated mathematical description in multistage processes.

## 4.3 Electrochemical Impedance Spectroscopy

In EIS, the input signal is a potential ($E_{\text{WE-RE}}$ or $U_{\text{C-A}}$) or current ($I_{\text{cell}}$), which is applied in the form of periodic cosine (sine) perturbation around a steady-state potential/current value. For the cosine perturbation, assuming a linear response, it will follow that:

$$\begin{aligned}\text{Input}: \Delta E_{\text{WE-RE}}(t) &= E_{\text{WE-RE}}(t) - E_{\text{WE-RE,SS}} = A\cos(\omega t) \\ &= \frac{A}{2}\left(e^{i\omega t} + e^{-i\omega t}\right) \qquad (53)\\ \text{Output}: \Delta I_{\text{cell}}(t) &= I_{\text{cell}}(t) - I_{\text{cell,SS}} \\ &= \frac{A}{2}\left(Y(\omega)e^{i\omega t} + Y(-\omega)e^{-i\omega t}\right) = A\cdot|Y|\cdot\cos(\omega t + \varphi) \qquad (54)\end{aligned}$$

Here, $Y(\omega)$ is a linear frequency response function (FRF), which corresponds to electrochemical admittance (reciprocal of electrochemical impedance ($Z^{-1}(\omega)$), $|Y|$ is an amplitude gain, $\varphi$ is a phase shift, and $\omega$ is an angular frequency in

rad $s^{-1}$. $Y(\omega)$ is defined as the ratio between output and input signals. This, it will follow from Eqs. 53 and 54 that:

$$Y(\omega) = |Y| \cdot e^{i\varphi} \tag{55}$$

Similarly, one can write for the electrochemical impedance:

$$Z(\omega) = |Z| \cdot e^{i\varphi} = \mathrm{Re}(Z) + i\mathrm{Im}(Z) \tag{56}$$

Keeping in mind that the electrochemical impedance is a complex number, it is common to plot its values as a Nyquist plot ($-\mathrm{Im}(Z)$ over $\mathrm{Re}(Z)$) or Bode plot ($\log|Z|$ and $\varphi$) over the log of frequency. Usually in these plots, the frequency ($f$) in $s^{-1}$ (Hz) is used instead of the angular frequency $\omega$, where:

$$\omega = 2\pi f \tag{57}$$

The frequencies of the input are changed between millihertz and megahertz. The whole impedance spectrum covers the whole range of frequencies.

Impedance spectroscopy was originally invented for the analysis of electrical circuits. Most electrochemical systems behave similarly to such equivalent circuits. The simplest example is an ideally polarizable electrode, which in terms of electrical circuit can be represented as a serial connection of an electrolyte resistance and a capacitance (Fig. 9a). In a more general case, an electrochemical reaction takes place at the electrode surface, causing a charge transfer resistance. For electroenzymatic reactions, the charge transfer resistance (resistance of electrochemical reaction) is accompanied by the resistance of enzymatic reactions. For example, in the case of DET (Eq. 34), these two resistances are connected in serial. The overall resistance of the electrochemical and biochemical reactions is denoted as $R_R$ in Fig. 9b. Additionally, the mass transfer of reactants or products contributes an additional resistance ($R_{MT}$). The reaction and mass transfer resistances are connected in parallel with double-layer capacitance. Furthermore, there is an ohmic resistance of the electrolyte, which is related to the ohmic drop in the electrolyte between the tip of the Luggin capillary and the WE.

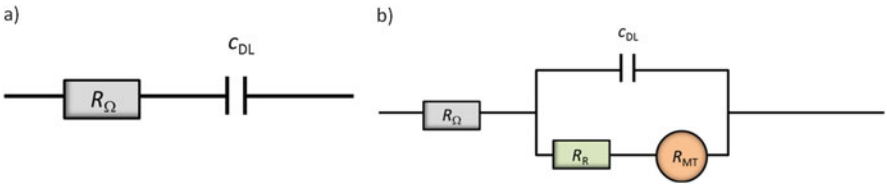


**Fig. 9** Equivalent circuits of (**a**) an ideally polarizable electrode (only electrolyte resistance and double-layer capacitance) and (**b**) a general electrochemical system showing electrolyte, reaction, and mass transfer resistance

The total impedance of the ideally polarizable electrode can be calculated as follows:

$$Z = \underbrace{R_\Omega}_{\substack{\text{Impedance of} \\ \text{electrolyte}}} - \underbrace{\frac{1}{i\omega c_{\mathrm{DL}}}}_{\substack{\text{Impedance of} \\ \text{double layer}}} \tag{58}$$

Here, it can be easily seen that:

$$\mathrm{Re}(Z) = R_\Omega \text{ and } \mathrm{Im}(Z) = -\frac{1}{\omega c_{\mathrm{DL}}} \tag{59}$$

The magnitude and the phase shift can be calculated accordingly:

$$|Z| = \sqrt{\mathrm{Re}(Z)^2 + \mathrm{Im}(Z)^2} \tag{60}$$

$$\varphi = a\tan\frac{\mathrm{Im}(Z)}{\mathrm{Re}(Z)} \tag{61}$$

The impedance of an ideally polarizable electrode is calculated based on Eqs. 58, 59, 60 and 61, with the double-layer capacitance value estimated from the CV of a porous enzymatic electrode (Fig. 8c) and the electrolyte resistance value based on a typical electrolyte resistance in a three-electrode set-up at pH 5 (~3 mΩ $m^2$) [33]. The calculated data are shown in Fig. 10 as Bode and Nyquist plots. As can be seen in Fig. 10a, at high frequencies, the behavior is dominated by the electrolyte resistance (the phase shift is 0° and the magnitude value corresponds to the assumed resistance value); at low frequencies, the behavior is dominated by the capacitive behavior, with a phase shift of −90° being typical for the capacitor. In case of an electroenzymatic reaction, in the absence of mass transfer resistance, the overall impedance will be as follows:

$$Z = \underbrace{R_\Omega}_{\substack{\text{Impedance of} \\ \text{electrolyte}}} + \underbrace{\frac{R_R}{1 - iR_R\omega c_{\mathrm{DL}}}}_{\substack{\text{Impedance of} \\ \text{double layer} \\ \text{and electroenzymatic} \\ \text{reaction in parallel}}} \tag{62}$$

where:

$$\mathrm{Re}(Z) = R_\Omega + \frac{R_R}{1 + R_R^2\omega^2 c_{\mathrm{DL}}^2} \tag{63}$$

$$\mathrm{Im}(Z) = -\frac{R_R\omega c_{\mathrm{DL}}}{1 + R_R^2\omega^2 c_{\mathrm{DL}}^2} \tag{64}$$

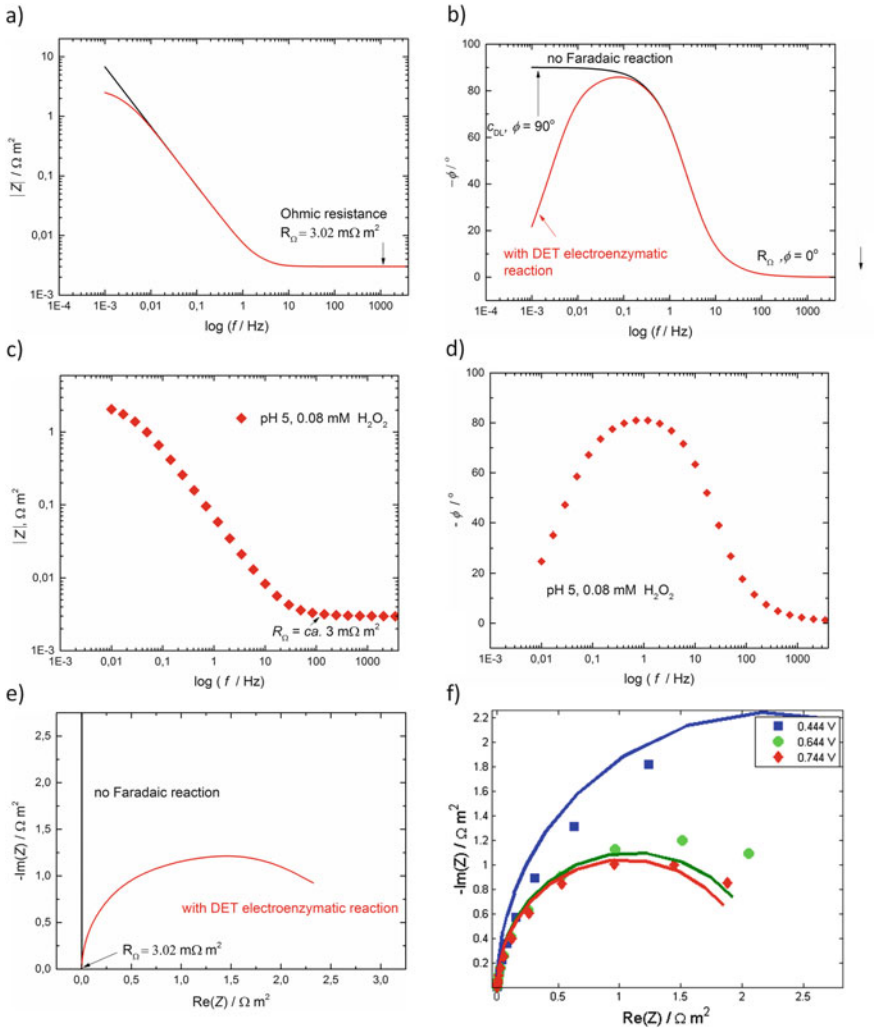


**Fig. 10** Calculated (**a**) magnitude and (**b**) phase shift of impedance of an enzymatic electrode without and with DET Faradaic reaction at $E = 0.744$ V; experimentally determined (**c**) magnitude and (**d**) phase shift of hydrogen peroxide reduction on an HRP-modified graphite RDE at $E = 0.744$ V; and calculated Nyquist plots using simplified Eqs. 63, 64 and 69 (**e**) and (**f**) a more rigorous overall impedance expression [33]. Conditions in (**e**) and (**f**): pH 5, 0.08 mM $H_2O_2$. (**f**) is reprinted from [33] with permission from Elsevier

The reaction impedance $R_R$ can be generally expressed as:

$$R_R = \left(\frac{\partial j}{\partial E}\right)^{-1} \tag{65}$$

For a simple electrochemical reaction:

$$\mathrm{ox} + \mathrm{e}^- = \mathrm{red} \tag{66}$$

with:

$$j = j_o\left(\exp\left(\frac{\alpha F}{\mathrm{RT}}(E - E^o)\right) - \exp\left(-\frac{(1-\alpha)F}{\mathrm{RT}}(E - E^o)\right)\right) \tag{67}$$

Assuming zero overpotential ($E - E^o = 0$), it can be easily shown that

$$R_R = \left(j_o \frac{F}{\mathrm{RT}}\right)^{-1} \tag{68}$$

For an electroenzymatic process, reaction impedance can be determined in a similar way from Eq. 37:

$$R_R = \left(\frac{\frac{\alpha F}{\mathrm{RT}} nF\Gamma_E k_2^2 c_R^2 k_{\mathrm{DE}}}{(k_2 c_R + k_{\mathrm{DE}}(K_M + c_R))^2}\right)^{-1} \tag{69}$$

Because Eq. 34 is derived by applying steady-state approximation, the expression in Eq. 69 will be strictly valid only for low frequencies (ω→0) and in the absence of mass transfer limitations. Still, for the sake of demonstration, it was used for calculation of the overall impedance of DET enzymatic electrode. The results in Fig. 10a and b show influence of the electroenzymatic reaction only in the low frequency range. The calculated data show good qualitative agreement with experimental data in Fig. 10c and d. The response of DET electroenzymatic electrodes in the Nyquist plot (Fig. 10e) shows the typical semicircle behavior that is characteristic for electrodes with a Faradaic reaction in the absence of mass transfer limitations. The more rigorously calculated DET impedance, based on the dynamic response of the DET electrode and taking into account mass transfer limitations, together with experimental data, are shown in Fig. 10f. This dependence is more complicated and involves constants of transient steps, which are not obvious in the simplified expression (Eq. 69) (for details, please see [33]). Therefore it has greater sensitivity for rate constants of steps, which show faster dynamics and can be used for their determination. In this respect, EIS shows higher sensitivity for model discrimination compared to stationary polarization. It could have been shown that only the model with Michaelis Menten kinetics can describe experimental data for all range of experimental conditions [33].

## *4.4 Parameter Determination*

In this section, the parameter determination based on discussed electrochemical methods is described. The main parameters of concern are kinetic rate constants

(enzymatic and electrochemical) and enzyme surface concentration. An additional parameter that appears to be important is the surface-to-volume area $a$, which accounts for the electrochemically active surface area in porous electrodes.

### 4.4.1 Kinetic Rate Constant Determination

The expression in Eq. 34 gives us a way to determine kinetic rate constants based on current potential measurements (e.g. from steady-state data for HRP-catalyzed hydrogen peroxide reduction at different concentrations, as shown in Fig. 11a). By replacing the reaction rate in Eq. 34 with the current density value divided by the number of electrons and Faraday's constant, it follows that:

$$\frac{nF}{j_{\mathrm{DET\_SS}}} = \frac{1}{\Gamma_E}\left[\frac{1}{k_e} + \frac{c_R(0,\mathrm{SS}) + K_M}{k_2 c_R(0,\mathrm{SS})}\right] \tag{70}$$

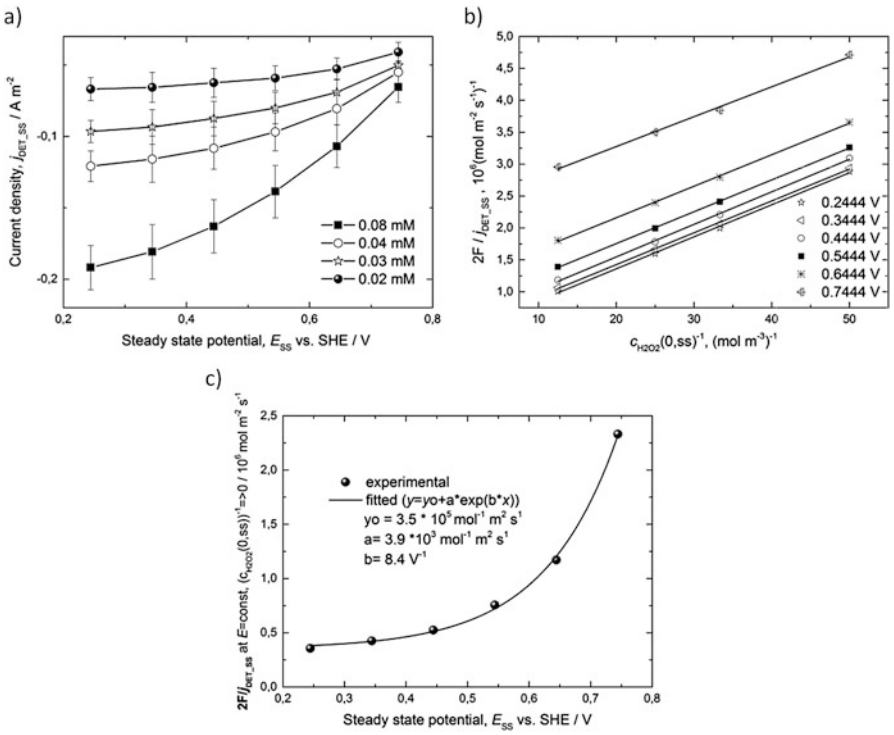


**Fig. 11** Determination of kinetic rate constants from stationary polarization measurements for an example of hydrogen peroxide reduction on HRP-modified graphite RDE. (**a**) Polarization curves for different hydrogen peroxide concentrations, (**b**) double reciprocal plot based on Eq. 70, and (**c**) nonlinear fit of intercept values from double reciprocal plot versus steady-state potential values. Conditions: pH 5, 0.1 M phosphate buffer, fixed delay 1 min, room temperature, rotation rate 400 rpm. (**a**) is based on data in [33]

By plotting the $\frac{nF}{j_{\mathrm{DET\_SS}}}$ (at $E_{\mathrm{ss}} = \mathrm{const}$) against the reciprocal value of the reactant concentration ($\frac{1}{c_R}$), one should obtain a family of straight lines (Fig. 11b), with slope equal to $\frac{1}{\Gamma_E}\frac{K_M}{k_2}$ and intercepts to $\frac{1}{\Gamma_E}\left[\frac{1}{k_\mathrm{e}} + \frac{1}{k_2}\right]$. Providing that the total enzyme surface concentration is known, one can easily obtain the $\frac{K_M}{k_2}$ ratio from the calculated slope value. Alternatively, by adopting the $\frac{K_M}{k_2}$ value based on homogeneous enzymatic catalysis, one can determine the total enzyme surface concentration. The values of intercept can be further plotted against the steady-state electrode potential values (Fig. 11c) because the $k_\mathrm{e}$ constant contains the potential dependence ( $k_\mathrm{e} = k_{\mathrm{e}0}\exp\left(-\frac{\alpha F}{\mathrm{RT}}\left(E_{\mathrm{SS}} - E^{o,\#}\right)\right)$. As expected, an exponential dependence is obtained. For the determination of kinetic parameters, nonlinear fit can be used (the nonlinear fit function and corresponding parameter values based on experimental data from Fig. 11a can be seen in Fig. 11c).

In this way, providing again that the total enzyme concentration value is known, the rate constants of the electrochemical step ($k_{\mathrm{e}0}$ and $\alpha$) and enzymatic step ($k_2$) can be obtained based on rate expression (Eq. 70).

Another strategy for the determination of rate constants (and other parameters) is based on global optimization of a large set of experimental data obtained under different operating conditions (concentrations, temperature, pH) and possibly by using different methods of measurements (steady-state and dynamic measurements; e.g. EIS). An objective function can be defined using the least square or weighted least square method (this should be the case when experimental data are not equally reliable). In the least square method, the sum of squared residuals is minimized, where the residuals are differences between the experimental values and the fitted values. In the weighted least square method, squared residuals are multiplied by corresponding weights. An example of the weighted least square objective function is [5]:

$$\sum_{j=1}^{m}\sum_{k=1}^{n}\left(j_{\mathrm{sim}}\left(c_{R,j}, E_k, p\right) - j_{\mathrm{exp}}\left(c_{R,j}, E_k\right)\right)^2 w_{jk} \tag{71}$$

where $p$ stands for all parameters that have to be determined (e.g. in Eq. 70, $\Gamma_E, k_{e0}$, $K_M, k_2$), $w_{jk}$ are weights, and subscripts "sim" and "exp" correspond to simulated and experimental data, respectively.

The comparison of model parameters obtained by the linearization method, followed by fitting of the exponential curve (Fig. 11a–c) and global optimization by using weighted least square objective function on the same set of experimental data, are shown in Table 4.

As can be seen in Table 4, the linearization approach gives similar values of model parameters. Some deviations can be ascribed to shortcomings of linearization by using the double reciprocal plot as well as neglecting the mass transfer limitations of the reactant. The latter effect has been taken into account into a model [33] that was used for calculation of the simulated data in a global optimization approach. The total enzyme surface concentration was a fitting parameter in the

**Table 4** Comparison of parameter values obtained using two different approaches

| Parameter ($p$) | Approach 1 (Fig. 13a–c) | Approach 2: Global optimization with objective function Eq. (71) [33] |
|---|---|---|
| $\alpha$ | 0.21 | 0.17 |
| $k_2$, $s^{-1}$ | 1.299 | 1.898 |
| $K_M$, mol $m^{-3}$ | 0.14 | 0.21 |
| $k_{e0}$, $s^{-1}$ | 33.72 | 37.80 |
| $\Gamma_E$, $10^{-9}$ mol $m^{-2}$ | 2.20[a] | 2.20 |

[a]Adopted value

global optimization method. As a starting value, the total enzyme surface concentration of 1.2 nmol $m^{-2}$ was used. This value was obtained from the slope of the linearized rate expression (Eq. 70), by adopting a $\frac{k_2}{K_M}$ value of $1.7 \times 10^4$ (mol $m^{-3}$)$^{-1}$ $s^{-1}$ for the enzyme in the solution, as suggested by Andreu et al. [6]. The total enzyme surface concentration in Approach 1 (Table 4) was assigned the same as in Approach 2.

### 4.4.2 Determination of Enzyme Surface Concentration

Obviously, knowledge of the total enzyme concentration value is essential for the determination of rate constants of both enzymatic and electrochemical steps. In some cases, the redox process at the enzyme redox site(s) can be evidenced electrochemically; therefore, the determination of the total enzyme surface concentration under electrochemical conditions appears possible. Typically, a cyclic voltammetry experiment is utilized in absence of reactive species and is called noncatalytic (nonturnover) cyclic voltammetry. In such an experiment, the redox center of the enzyme is oxidized/reduced electrochemically during the potential sweep, showing corresponding redox peaks in the cyclic voltammogram. As an example, a cyclic voltammogram of cytochrome c peroxidase modified pyrolithic graphite electrode is shown in Fig. 12 [44, 45].

As can be seen in Fig. 12, an almost reversible redox peak at a potential assigned to the reduction potential of cytochrome c peroxidase compound I appears. At low enzyme surface coverage, this redox peak can be masked by the electrode capacitive contributions, which might necessitate a background current subtraction (e.g. in [46]). The enzyme's total concentration can be calculated from the charge under the redox peak, by assuming a number of exchanged electrons in accordance to the following [33]:

$$\Gamma_E = \frac{\int_{E_1}^{E_2} j \cdot \mathrm{d}E}{nF \cdot v} \tag{72}$$

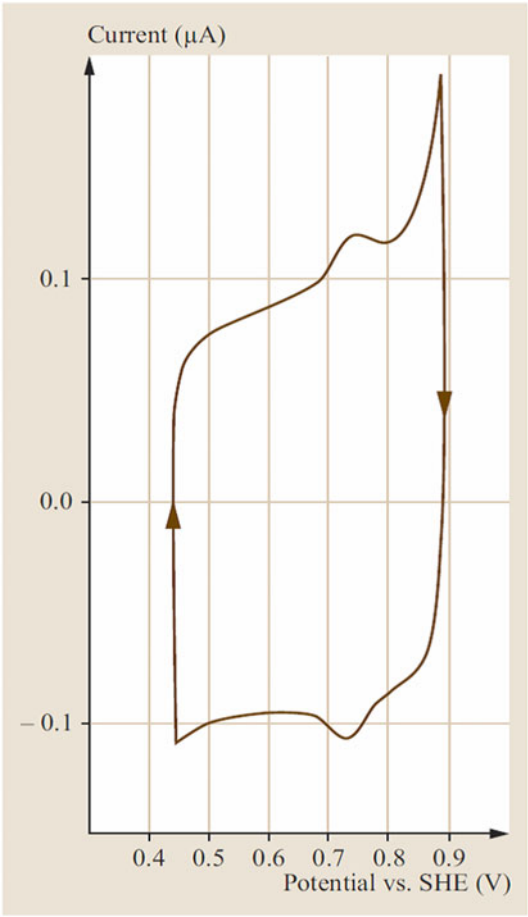


**Fig. 12** Cyclic voltammogram of cytochrome c peroxidase modified pyrolithic graphite electrode in 20 mM phosphate buffer, pH 6.1, 4°C. Reprinted from [33] with permission from Springer Verlag

Here, $E_1$ and $E_2$ are potential limits of cyclic voltammetry experiment, $n$ is the number of exchanged electrons, and $v$ is the sweep rate in V $s^{-1}$. The total enzyme surface concentration of cytochrome c peroxidase on modified pyrolithic graphite electrode, assuming the $2e^-$ process, was determined to be 6.2 pmol $cm^{-2}$.

Usually, there is no evidence of enzyme redox activity on the electrode surface in the absence of a reactive species. In such a case, nonturnover voltammetry is not helpful for the total enzyme surface concentration determination. Also, as demonstrated in an example of stationary polarization, total enzyme surface concentration cannot be directly obtained from the experimental polarization curves. The problem can be circumvented by the combination of stationary polarization and EIS measurements. As it follows from Eq. 69, the real part of the EIS at low frequencies (which corresponds to the diameter of the semicircle) depends on kinetic rate constants and total enzyme surface concentration. Therefore, the combination of

these two methods (or other electrochemical methods) can enable "direct" determination of the enzyme surface concentration.

An estimation of the total enzyme surface concentration can be obtained by assuming the same kinetic activities as for enzymes under homogenous conditions, where the well-established values exist in literature. This approach was discussed by Andreu et al. [6]. They obtained $\Gamma_E$ values in the range from 0.09 to 0.14 pmol $cm^{-2}$ for pH range from 4.1 to 8 and for HRP, by adopting $\frac{k_2}{K_M}$ value of $1.7 \times 10^4$ $(mol\ m^{-3})^{-1}\ s^{-1}$ for enzymes in the solution. The authors commented that the obtained values represent lower limits of the total enzyme surface concentrations because the activity of immobilized enzymes is probably reduced compared to the homogenous case of enzymes in the solution. These values are only approximately 1% of the calculated value of a fully packed enzyme monolayer of approximately 10 pmol $cm^{-2}$ based on enzyme crystallographic data [6]. The authors concluded that the real value of the total enzyme surface concentration is somewhere between approximately 0.1 and 10 pmol $cm^{-2}$, where the values closer to the lower limit are supported by the absence of nonturnover activity in cyclic voltammetry. Other values reported in the literature for this enzyme are in the range from 0.1 to 40 pmol $cm^{-2}$ [6, 47, 48].

### 4.4.3 Other Parameters

Another parameter of interest is the surface-to-volume area $a$, which appears important in porous enzymatic electrodes. In DET, the parameter $a$ depends on the internal surface area of electron conductive support in contact with an enzyme. This can be estimated based on electron conductive material loading and BET surface area, as well as the thickness of the porous electrode. Carbon nanomaterials, which are often employed as electroconductive supports, have BET surface areas in the range between 200 and 600 $m^2\ g^{-1}$. For Vulcan XC 72, the BET surface area is 250 $m^2\ g^{-1}$. The addition of binder materials, which are necessary for porous electrodes, might reduce this area significantly. In fuel cell research, a BET area reduction up to ten times, depending on binder-to-carbon ratios, was observed [49]. Assuming a similar effect of the binder in the present case and Vulcan XC 72 loading of 3.0 mg $cm^{-2}$ and 53-μm [5] electrode thickness, one can calculate the internal surface area of $1.4 \times 10^7$ $m^2_{act}/m^3_{geo}$. Assuming further similar coverage as in the case of the flat electrode (~1% of the full monolayer) and molecular weight of HRP of 44 kDa, one can calculate the enzyme loading of such an electrode of approximately 33 mg $cm^{-2}_{geo}$. For comparison, the value that was obtained in [5] by using model-based analysis was approximately 6 mg $cm^{-2}_{geo}$. The difference can be a consequence of overestimation of the internal surface area of the carbon support. However, it may also indicate that even lower enzyme coverage than on the flat surface is obtained in porous electrodes.

# 5 Toward the Development of Electrobiotechnological Processes

This section reviews some recent advances in the preparation of enzyme-modified electrodes. This mainly concerns research activities where the enzyme co-factor is an inherent part of the enzyme. Additionally, some challenges in the electrochemical regeneration of soluble co-factors (co-substrates; e.g. NAD, NAD(P)) are discussed.

## *5.1 Development of Enzyme-Modified Electrodes*

A technical enzymatic electrode can be defined as a composite structure containing different layers such as a catalyst layer and/or diffusion layer and current collectors. Thereby, enzymatic catalysts are integrated into the catalyst layer by immobilization or by entrapment behind, for example, a dialysis membrane. Although the latter approach is simpler [50], the performance of such electrodes is lower (~50 μA $cm^{-2}$ [50] compared to ~700 μA $cm^{-2}$ [51] for the case of enzymatic electrodes employing hydrogenases). In Fig. 13a, a schematic representation of an enzymatic fuel cell containing two porous enzymatic electrodes is shown. The anode comprises a porous catalyst layer containing electron conductive nanoparticles, a mediator, binder, and the enzyme GOx (Fig. 13c) [40]. Stainless steel was used as a current collector. The cathode is a so-called gas diffusion electrode, with a catalyst layer applied on the gas diffusion layer. The graphite flow field serves as a current collector. The catalyst layer on the cathode side contains electron conductive nanoparticles, binder, and enzymes.

Both anode and cathode catalyst layers contain porous electron conductive matrixes, which are formed out of carbon, gold nanoparticles, or polymer materials [51–54]. Most recent studies have concentrated on the use of carbon nanomaterials [54]. To form porous structures, carbon nanoparticles have to be pressed in pallets or bonded using a suitable binder. Such binder materials include polyvinylidene fluoride (PVDF) and gelatin [2]. PVDF is a highly nonreactive fluoropolymer that is chemically inert in the presence of different solvents, acids, and bases, while gelatin is a biocompatible natural polymer. In both cases, the binder is mixed with electron conductive nanomaterial and a mediator (for MET electrodes only) and left to dry. This procedure is applicable for immobilized mediators supplied as nanomaterials or polymers, as well as for dissolved mediators.

The choice of mediator depends on the enzyme cofactor, as well as on the purpose of the electroenzymatic system. For example, soluble mediators might complicate downstream processing of the reaction mixture; they are less preferred for implantable devices (e.g. enzymatic fuel cells for in vivo operation) [2]. In combination with GOx (FAD cofactor), different mediators have been used. Some examples are ferrocene [55], tetrathiafulvalene (TTF) [35, 43], 8-hydroxyquinoline-5-sulfonic

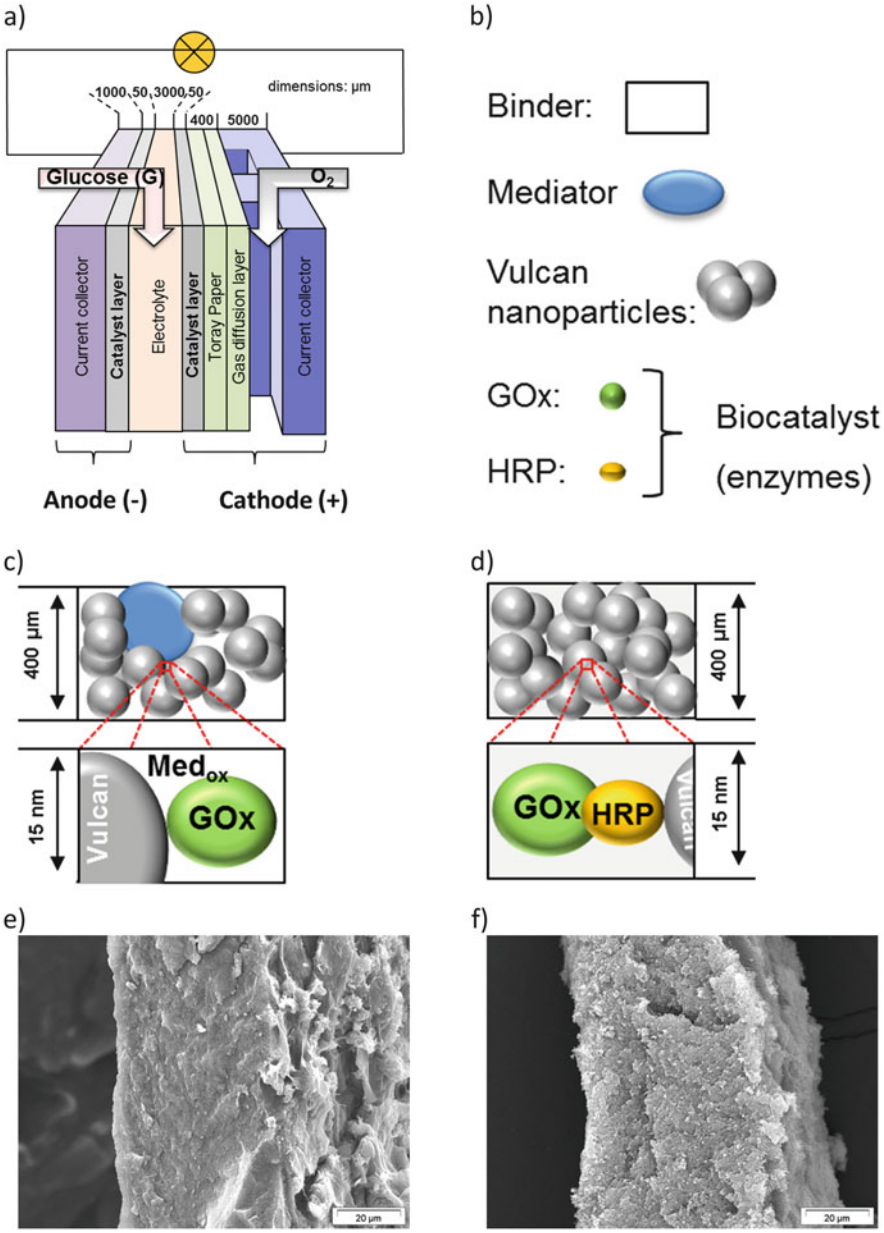


**Fig. 13** (**a**) A schematic representation of an enzymatic fuel cell, (**b**) legend, (**c**) structure of the catalyst layer on the anode side, and (**d**) a catalyst layer structure on the cathode side, and SEM cross-sections of enzymatic electrodes with (**e**) Vulcan/Gelatin binder and (**b**) Vulcan/PVDF binder. (**a**,**b**,**c**) were reprinted from [40], (**e** and **f**) were reprinted from [39]

acid (HQS) [24], and Os redox hydrogels [19]. Beyond these mediators, Os hydrogels with redox centers attached to a polymer backbone exhibited the best performance. Their disadvantages include complicated synthesis procedures and toxicity issues associated with Os. A TTF mediator has been used either alone [26, 35, 40] or in combination with tetracyanoquinodimethanide (TCNQ), forming a charge transfer complex (CTC) that then acts as a mediator [43, 56–58]. Although CTC is electronically conductive, TTF has negligible conductivity, which is the reason why it is usually integrated into the electron conductive matrix. CTC has shown excellent performances in biosensor electrodes, high oxygen tolerance, and remarkable stability under continuous operation [56]. A further advantage is that enzymatic electrodes based on CTC do not require complicated modification procedures; they can be prepared just by mixing the respective components [59]. CTC is commercially available and has high electronic conductivity, which is beneficial for lowering the ohmic resistance within the electrode layer. The morphology of the CTC crystals can be tuned by variation of the experimental conditions [59]. They can be also prepared as nanoparticles. These strategies can be applied to tune the catalytic properties of the CTC and/or to increase the catalytically active surface area. Both TTF and TCNQ have low toxicity, which is attributed to their low solubility in water and physiological fluids. Although CTC can be employed without an electron conductive material due to its own electron conductivity, the addition of carbon nanoparticles improves the electrode performance [43].

The enzymes can be immobilized into the porous matrix together with the binder or separately. The first possibility is convenient when gelatin is used as a binder, whereas the second one is preferred when PVDF is used as a binder. (PVDF has to be dissolved in an organic solvent before mixing it with electron conductive nanoparticles and a mediator, which might not be compatible with enzymes; additionally, during drying of the porous matrix, the enzyme might denature.) In both described cases, the enzyme immobilization is physical. If enzymes are physically adsorbed in a PVDF bonded carbon nanoparticle porous matrix, only a weak interaction between a support and an enzyme is assumed. In this way, enzymes can be "wired" to different electron conducting materials (e.g. gold and carbons). Over the long term, this method of immobilization shows some loss of stability due to enzyme leaching. If the enzymes are physically immobilized by entrapment into a gel matrix formed by gelatin (collagen and polysaccharides can also be used), the stability of such electrodes is improved; however, the enzyme activity might be influenced. Because gelatin is soluble in water, to assure the mechanical stability of the catalyst layer, it has to be cross-linked with glutaraldehyde. This step improves the stability but reduces the activity of enzymes. Stability can be also improved by the covalent attachment of enzymes to the electrode surface. In this case, the electrode has to be functionalized with surface groups favoring covalent attachment with surface groups of enzymes.

The enzyme immobilization procedure has significant influence on activity of porous enzymatic electrodes. The comparison of two immobilization procedures defined by use of two binders (PVDF and gelatin) in an example of DET and MET enzymes is shown in Fig. 14. For the DET enzyme, a PVDF procedure where

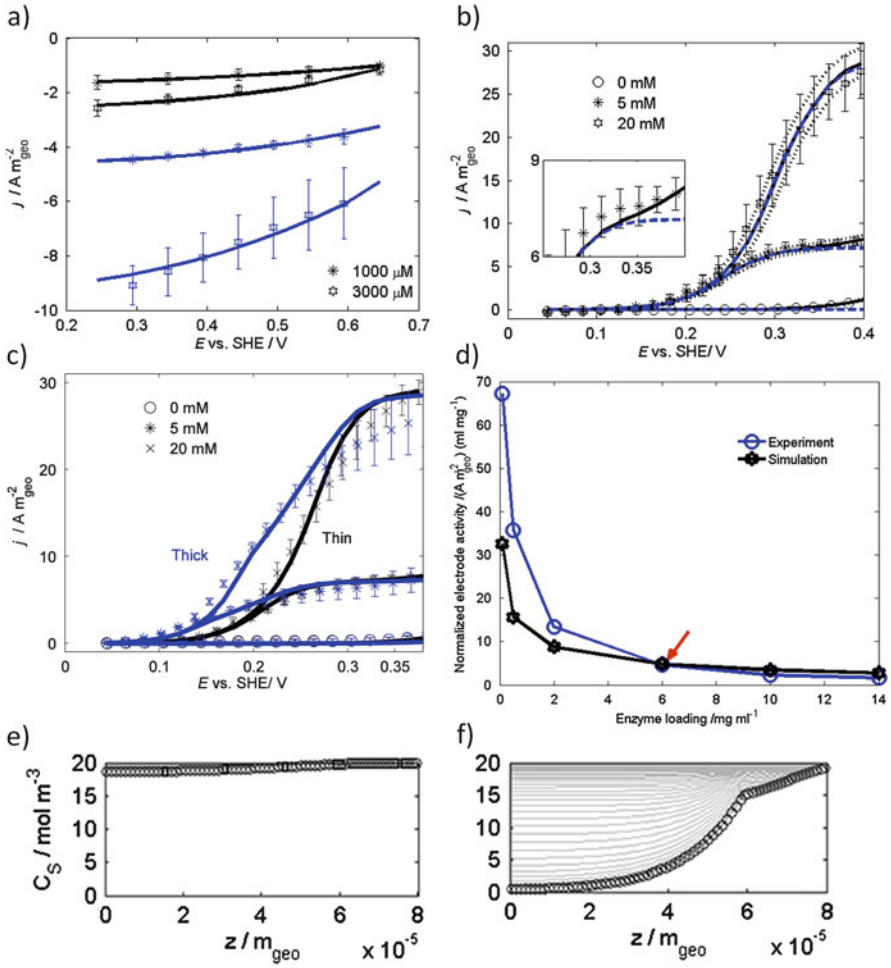


**Fig. 14** Influence of the immobilization procedure (binder) on activities of enzymes showing (**a**) DET mechanism (black lines = gelatin binder, blue line = PVDF binder; reprinted from [5] with permission from Elsevier) (**b**) MET mechanism (PVDF binder; reprinted from [35] with permission from Elsevier) and (**c**) MET mechanism (gelatin binder) at two different thicknesses of the porous electrodes (reprinted from [60] with permission from the author); (**d**) influence of enzyme loading on normalized activity of MET electrode and simulated concentration profiles along the spatial coordinate at two different enzyme loadings and 0.4 V (**e**) low enzyme loading (0.1 mg $mL^{-1}$); (**f**) high enzyme loading (14 mg $mL^{-1}$; reprinted from [35] with permission from Elsevier). Conditions: (a) $H_2O_2$ reduction on gelatin or PVDF/Vulcan/HRP enzymatic electrodes, pH 5, room temperature, stationary polarization (b) glucose oxidation on PVDF/Vulcan/GOx, and (c) on gelatin/Vulcan/GOx enzymatic electrodes, pH 7, 37°C, stationary polarization

enzymes are only physically adsorbed is more beneficial in the whole range of studied overpotentials (Fig. 14a). For MET enzymes, the limiting current region is almost independent on the electrode preparation procedure, while the kinetic region

is significantly influenced. Additionally, the kinetic region is dependent on the catalyst layer thickness (Fig. 14c). Comparing the performances of thick MET electrodes prepared using PVDF (59-μm thickness) and gelatin (65-μm thickness) binders, the gelatin electrode has better performance in the kinetic region (at lower overpotentials) [35]. The performance of a thick PVDF electrode (59-μm thickness) is similar to the performance of a thin gelatin electrode (19-μm thickness). Based on modeling results, the PVDF procedure "offers" more active DET enzymes than the gelatin procedure [5, 35]. This can be rationalized by enzyme agglomeration in the presence of gelatin and the cross-linking agent glutaraldehyde [39]. The formation of enzyme agglomerates decreases the number of DET enzymes in contact with the electrode surface, leading to lower activity. An additional reason for the observed differences is mass transport limitation. Based on modeling results, a DET gelatin electrode is less limited by mass transport than a DET PVDF electrode due to the lower number of active enzymes.

In MET electrodes, the differences in the kinetic region can be caused by differences in either mediator or enzyme concentrations. According to modeling results, a change in mediator concentration causes an almost parallel shift of the polarization curve on the potential scale, while a change in enzyme concentration leads to branching of the polarization curves [35]. The former effect describes the behavior of MET electrodes with respect to the preparation procedure and electrode thickness. The results indicate a lower concentration of the mediator in the MET PVDF electrode compared to an MET gelatin electrode of similar thickness. At more positive overpotentials, the activity depends on the enzyme concentration and mass transfer limitations. Although the thick MET gelatin electrode has a larger number of enzymes, it is more limited by mass transport; this leads to a lower level of enzyme utilization and finally to a similar performance compared to the thin electrode at more positive overpotentials. With an increase of enzyme loading, the normalized electrode activity is decreasing (Fig. 14d). One of reasons is the depletion of reactants along the catalyst layers (Fig. 14e, f) [35].

## *5.2 Electrochemical Regeneration of Soluble Co-Factors*

Many enzymes of technological interest are dependent on soluble co-factors, such as nicotinamide adenine dinucleotide (NAD) and nicotinamide adenine dinucleotide phosphate (NADP) in their oxidized ($NAD^+$, $NADP^+$) or reduced forms (NADH, NADPH) [61]. The regeneration of these co-factors is of paramount interest with respect to the technical applications of these enzymes. In a most favorable case, their electrochemical regeneration occurs at low overpotentials, showing fast kinetics and high selectivity towards enzymatically active forms of these co-factors as well as high current efficiency. In reality, these conditions are not easily satisfied. The equilibrium electrode potential of the $NAD^+$/NADH reaction (−0.32 V SHE) is close to the equilibrium electrode potential of the hydrogen reaction $2H^+/H_2$ (−0.414 V SHE). Considering the fast kinetics of the

hydrogen reaction on most electrode materials, it can be expected that the current efficiency for $NAD^+$($NADP^+$) reduction will be significantly lowered. It was also reported that the direct reduction of $NADP^+$ leads to one electron charge transfer and formation of a radical NADP form, followed by dimerization to an enzymatically inactive dimer form [62]. Similarly, the direct electrochemical oxidation of NADH takes place only at very high overpotentials; it is further complicated by side reactions, such as the direct anodic oxidation of reactants and electrode fouling [61]. More promising than the direct electrochemical regeneration is a mediated regeneration. A number of different mediators has been reported so far (see e.g. [33] and references therein). Most of these mediators support electrochemical regeneration of either oxidized or reduced forms of soluble co-factors. However, in few cases, electrocatalytic systems were able to regenerate both oxidized and reduced forms [33]. For example, a pyrolytic graphite edge electrode modified by a hydrophilic domain of mitochondrial NADH ubiqinone oxidoreductase was able to regenerate both forms of NAD co-factor at low overpotentials. The drawbacks of this approach were low stability and current densities. Similar findings were reported for electropolymerized neutral red [63]. In this first report, no enzymatic reaction was coupled with the regeneration system. In a later report by Arechederra et al. [64], the same polymer was used for $NAD^+$ and NADH regenerations in a rechargeable ethanol-fueled biobattery.

Other reported mediator modified electrodes support regeneration of either an oxidized or reduced form of a co-factor. Poly(methylene green) was reported as a highly efficient mediator for NADH oxidation by several groups [61, 65–67]. Poly (methylene green) modified carbon nanotubes showed high electrocatalytic activity for NADH oxidation, reaching current densities up to 5 mA $cm^{-2}$ at overpotentials of approximately 0.5 V [66]. Kochius et al. [61] studied different mediators for NADH oxidation. As a most promising candidate, 2,2′-azino-bis-(3 ethyl-benzothiazoline-6-sulfonic acid) (ABTS) was identified. High substrate conversions and high space time yields were achieved. The ABTS also showed remarkable stability during prolonged cycling. Drawbacks of this mediator include the high overpotential required for the NADH oxidation as well as problems related to its separation out of the reaction mixture.

$NAD^+$ and $NADP^+$ were reduced to NADH and NADPH using (pentamethylcyclopentadienyl- 2,2V-bipyridine aqua) rhodium (III) as a mediator [68]. The regeneration was performed in a packed bad reactor with 100% selectivity and conversion. A high space-time yield of 500–1,000 g $dm^{-3}$ $day^{-1}$ was achieved. The authors also suggested downstream processing (including ion exchange) to remove the mediator, nanofiltration to remove the buffer, and finally freeze-drying of the reduced nicotinamide coenzyme.

Composite electrodes containing a Ru(III) complex and single-walled carbon nanotubes were reported to be active in the regeneration of electrochemically active 1,4 NADH [69] Also, it was shown that traditional carbon electrodes under certain conditions (high overpotentials) almost exclusively (98% yield) formed enzymatically active 1,4-NADH forms [70].

Catalytic systems requiring NADH (NADPH) co-factor and additional substrates such as oxygen are especially challenging. This is the case in biocatalysis with monooxygenases, where the oxygen sensitivity of the mediator as well as possible direct electrochemical oxygen reduction have to be considered [71]. From this work, the authors concluded that the combination of an oxygen-independent enzyme reaction with an electrochemical reaction is more advisable. Therefore, a mediated electroenzymatic process to regenerate the NADPH in combination with a reaction catalyzed by flavin-dependent-OYE (old yellow enzymes) was investigated. High productivities up to 2.27 mM product $h^{-1}$ in combination with approximately 90% electron transfer efficiency were measured [72].

In addition to approaches that concentrate on a search and optimization of a mediator for co-factor regeneration, some groups have attempted to replace natural co-factors with artificial redox mediators. For example, Cekic et al. [73] replaced NADPH with different artificial redox mediators in combination with P450cin monooxygenase. It was shown that cobalt sepulchrate, phenosafranine, safranine T, FAD, and FMN enabled artificial electron transfer from the platinum electrode to P450cin via the redox partner protein cindoxin. The highest product formation of $6.50 \pm 0.60$ nmol (product) and $(P450)^{-1}$ $min^{-1}$ $cm^{-2}$ was achieved using cobalt sepulchrate. An interaction between proteins and artificial redox mediators can be further tuned by protein engineering, as shown by Belsare et al. [3]. Furthermore, computational studies can provide a deeper understanding of the interaction of a mediator with the amino acids of an enzyme [74].

## 6 Conclusions

The chapter summarized the fundamentals of enzyme employment in electrobiotechnological applications. The most common enzyme cofactors and mechanisms of electron transfer between an enzyme and an electrode have been introduced. The basics of thermodynamics of half-cell reactions and cell reactions were described, including the meanings of standard electrode potential, electrode potential at specified pH value, standard cell potential, and open circuit potential. Tables with Gibbs free energies of formation of selected substances and selected half-cell potential values at pH 7 for some selected examples were given. Kinetic expressions for DET and MET mechanisms were introduced and the overall reaction rate in an example of a DET mechanism were discussed. The balance equations necessary for mathematical descriptions of electroenzymatic processes on flat and porous enzymatic electrodes were introduced. This was followed by descriptions of selected electrochemical methods of study, such as stationary polarization, cyclic voltammetry, and electrochemical impedance spectroscopy. The descriptions of methods was accompanied by selected examples relevant to

electrobiotechnological applications. It was also shown how kinetic and electrochemical rate constants can be determined from the measurements. The determination of total enzyme surface concentration was also discussed. Finally, some methods for the preparation of porous electroenzymatic electrodes and regeneration of soluble co-factors were introduced.

It was demonstrated that the electrochemical methods, combined with proper mathematical descriptions, can provide significant insights on the reasons limiting the overall electrode behavior, contributing to better system design. However, to make these models more realistic, additional porous electrode characterizations are necessary. For example, there is a little knowledge about the real structure of porous enzymatic electrodes. Currently, only a few studies offer enough data on electrode thicknesses, porosity, and real surface area, while the data on realistic enzyme and mediator distributions are lacking. Most studies are not concerned with enzyme/mediator/nanoparticle loadings or their utilization. Current results point out very low enzyme utilization in most publications. Because enzymes are catalysts which have to be produced and thus also create some waste, this factor has to be considered in the future if enzymatic systems are ever going to be competitive with fermentation systems. For systems with a main focus on material production, the characterization of product distribution is of paramount interest. Currently, most of these studies consider quite diluted systems. This is a significant drawback because it significantly increases the separation cost and the amount of waste liquids. To fully develop the potential of electrobiotechnological systems, electroenzymatic syntheses in more concentrated solutions have to be demonstrated. As was shown, the choice of mediator is not always simple, especially if additional substrates (e.g. oxygen) are required, as in the case of monooxygenases. Recent works indicate that the properties of enzymes toward artificial mediators can be further tuned by protein engineering. This direction will be hopefully be further explored in the future. To develop sustainable processes, issues related to the separation (recycling) and toxicity of selected mediators have to be carefully considered. Finally, to push forward new and exciting electrobiotechnological applications, more intensive interactions between different disciplines—including electrochemistry, biology, bioelectrochemistry, material science, and reaction engineering—are strongly recommended.

## Appendix: List of Symbols

| | |
|---|---|
| $A$ | Amplitude (V) |
| $a$ | Internal active surface area ($m_{act}^2\ m_{geo}^{-3}$) |
| $A_{geo}$ | Geometrical surface area of electrode ($m_{geo}^2$) |
| $c$ | Volumetric concentration (mol $m^{-3}$) |
| $c_{DL}$ | Double layer capacitance (F $m^{-2}$) |
| $D$ | Diffusion coefficient of species ($m_{geo}^2\ s^{-1}$) |
| $E$ | Electrode potential (V) |

| | |
|---|---|
| F | Faraday's constant = 96,485 (C $mol^{-1}$) |
| $f$ | Frequency (Hz) |
| $G$ | Flow rate ($m^3$ $s^{-1}$) |
| $g_k$ | Diffusion flux ($k$ = 1,2,3) (mol $m_{geo}^{-2}$ $s^{-1}$) |
| $I$ | Current (A) |
| $i$ | Imaginary number |
| Im($Z$) | Imaginary part of electrochemical impedance $Z$ ($\Omega$ $m^2$) |
| $j$ | Current density (A $m_{geo}^{-2}$) |
| $k_1$, $k_m$ | Reaction constants of enzyme substrate ($m^3$ $mol^{-1}$ $s^{-1}$/$m^2$ $mol^{-1}$ $s^{-1}$) and enzyme mediator reactions |
| $k_{ei}$ | Kinetic constant of the ($s^{-1}$) Electrochemical reaction ($i$ = 1,2) |
| $K_M$ | Michaelis-Menten constant (mol $m^{-3}$) |
| $L$ | Catalyst layer thickness ($m_{geo}$) |
| $n$ | Number of electrons |
| $P$ | Power density (W $m^{-2}$) |
| $r$ | Reaction rate (mol $s^{-1}$ $m^{-2}$) |
| R | Universal gas constant = 8.314 (J $mol^{-1}$ $K^{-1}$) |
| $R_\Omega$ | Electrolyte resistance ($\Omega$ $m^2$) |
| Re($Z$) | Real part of electrochemical impedance $Z$ ($\Omega$ $m^2$) |
| $T$ | Temperature (K) |
| $U$ | Cell potential (V) |
| $v_k$ | Average molar velocity ($k$ = 1,2,3) (m $s^{-1}$) |
| w | Rotation rate of rotating disc electrode (rad $s^{-1}$) |
| Y | Linear frequency response function ($\Omega^{-1}$ $m^{-2}$) |
| \|Z\| | Magnitude of electrochemical impedance $Z$ ($\Omega$ $m^2$) |
| $Z$ | Electrochemical impedance ($\Omega$ $m^2$) |
| $z_k$ | Space coordinate ($k$ = 1,2,3) |
| $v$ | Sweep rate (V $s^{-1}$) |

## *Greek*

| | |
|---|---|
| $\nu$ | Stoichiometric coefficient |
| $\eta$ | Overpotential (V) |
| $\varphi$ | Phase shift ($^o$) |
| $\Gamma$ | Surface concentration (mol $m^{-2}$) |
| $\eta_i$ | Efficiency (i = th, ec,fuel) |
| $\Delta_f G_i^o$ | Standard Gibbs free energies of formation of component "i" (kJ $mol^{-1}$) |
| $\Delta_r G^o$ | Standard Gibbs free energy change of reaction (kJ $mol^{-1}$) |
| $\Delta_r H^o$ | Standard enthalpy change of reaction (kJ $mol^{-1}$) |
| $\phi_E$, $\phi_I$ | Potentials of electron-and ion- conducting phases, respectively (V) |
| $\gamma_E$, $\gamma_I$ | Electron-and ion conductivities (S $m_{geo}^{-1}$) |
| $\alpha$,$\beta$ | Transfer coefficients of electrochemical steps |
| $\delta$ | Diffusion layer thickness ($m_{geo}$) |
| $\varepsilon$ | Void fraction ($m^3 m_{geo}^{-3}$) |
| $\iota$ | Local current density (A $m_{act}^{-2}$) |
| $\omega$ | Angular frequency (rad $s^{-1}$) |

## *Super- and Sub-scripts*

| | |
|---|---|
| A,C,cell | Anode, cathode and cell respectively |
| act, geo | Active and geometrical respectively |
| CL, DL | Catalyst layer and diffusion layer respectively |
| e0 | Electrochemical reaction step |
| ec | Electrochemical |
| I, E | Ion and electron conducting phase respectively |
| o | Standard conditions |
| o,# | At pH 7 |
| Ohm | Ohmic |
| ox,red | Oxidized and reduced states respectively |
| S | Substrate |
| sim, exp. | Simulation and experiment respectively |
| SS | Steady state |
| th | Thermodynamic |

## *List of Abbreviations*

| | |
|---|---|
| A | Anode |
| Ag/AgCl | Silver/silver chloride reference electrode |
| C | Cathode |
| CC | Current collector |
| CE | Counter electrode |
| CL | Catalyst layer |
| DET | Direct electron transfer |
| DET_SS | Direct electron transfer steady state |
| E | Enzyme |
| EM | Enzyme mediator complex |
| ES | Enzyme substrate complex |
| FAD | Flavin adenine dinucleotide |
| FMN | Flavin mononucleotide |
| GOx | Glucose oxidase |
| HRP | Horseradish peroxidase |
| Int | Intermediate |
| Medi (i = ox,red) | Oxidized and reduced forms of a mediator |
| MET | Mediated electron transfer |
| NAD | Nicotinamide adenine dinucleotide |
| NADP | Nicotinamide adenine dinucleotide phosphate |
| P | Product |
| RE | Reference electrode |
| RH | Organic substrate |
| S | Substrate |
| SAMs | Self-assembled monolayers |
| SCE | Saturated calomel electrode |
| SHE | Standard hydrogen electrode |
| WE | Working electrode |

## References


1. Copeland RA (2000) Enzyme reactions with multiple substrates. In: Enzymes: a practical introduction to structure, mechanism, and data analysis, 2nd edn. Wiley, New York, pp 350–366
2. Vidakovic-Koch T, Sundmacher K (2017) Porous electrodes in bioelectrochemistry. In: V P (ed) Encyclopedia of interfacial chemistry: surface science and electrochemistry, Elsevier, Amsterdam
3. Belsare KD et al (2017) Directed evolution of P450cin for mediated electron transfer. Protein Eng Des Sel 30(2):119–127
4. Habermüller K, Mosbach M, Schuhmann W (2000) Electron-transfer mechanisms in amperometric biosensors. Fresenius J Anal Chem 366(6):560–568
5. Do TQN et al (2014) Mathematical modeling of a porous enzymatic electrode with direct electron transfer mechanism. Electrochim Acta 137:616–626
6. Andreu R et al (2007) Direct electron transfer kinetics in horseradish peroxidase electrocatalysis. J Phys Chem B 111(2):469–477
7. Gupta G et al (2011) Direct electron transfer catalyzed by bilirubin oxidase for air breathing gas-diffusion electrodes. Electrochem Commun 13(3):247–249
8. Léger C et al (2002) Effect of a dispersion of interfacial electron transfer rates on steady state catalytic electron transport in [NiFe]-hydrogenase and other enzymes. J Phys Chem B 106 (50):13058–13063
9. Tasca F et al (2008) Direct electron transfer at cellobiose dehydrogenase modified anodes for biofuel cells. J Phys Chem C 112(26):9956–9961
10. Zimmermann H et al (2000) Anisotropic orientation of horseradish peroxidase by reconstitution on a Thiol-modified gold electrode. Chem Eur J 6(4):592–599
11. Vidaković-Koch T et al (2011) Impact of the gold support on the electrocatalytic oxidation of sugars at enzyme-modified electrodes. Electroanalysis 23(4):927–930
12. Courjean O, Gao F, Mano N (2009) Deglycosylation of glucose oxidase for direct and efficient glucose electrooxidation on a glassy carbon electrode. Angew Chem 121(32):6011–6013
13. Bartlett PN, Al-Lolage FA (2017) There is no evidence to support literature claims of direct electron transfer (DET) for native glucose oxidase (GOx) at carbon nanotubes or graphene. J Electroanal Chem
14. Alberty RA (1993) Thermodynamics of reactions of Nicotinamide adenine dinucleotide and Nicotinamide adenine dinucleotide phosphate. Arch Biochem Biophys 307(1):8–14
15. Krebs HA, Kornberg HL (1957) Energy transformations in living matter. Springer-Verlag Berlin Heidelberg, Berlin
16. Reiger PH (1994) Electrochemistry.2nd edn. Springer Science+Business Media, Dordrecht
17. Armstrong FA, Hirst J (2011) Reversibility and efficiency in electrocatalytic energy conversion and lessons from enzymes. Proc Natl Acad Sci 108(34):14049–14054
18. Togo M et al (2007) An enzyme-based microfluidic biofuel cell using vitamin K3-mediated glucose oxidation. Electrochim Acta 52(14):4669–4674
19. Mano N, Mao F, Heller A (2002) A miniature biofuel cell operating in a physiological buffer. J Am Chem Soc 124(44):12962–12963
20. Chen T et al (2001) A miniature biofuel cell. J Am Chem Soc 123(35):8630–8631
21. Kim H-H et al (2003) A miniature membrane-less biofuel cell operating under physiological conditions at 0.5 V. J Electrochem Soc 150(2):A209–A213
22. Willner I et al (1998) Biofuel cell based on glucose oxidase and microperoxidase-11 monolayer-functionalized electrodes. J Chem Soc Perkin Trans 2(8):1817–1822
23. Kuwahara T et al (2007) Properties of the enzyme electrode fabricated with a film of polythiophene derivative and its application to a glucose fuel cell. J Appl Polym Sci 104 (5):2947–2953
24. Brunel L et al (2007) Oxygen transport through laccase biocathodes for a membrane-less glucose/O2 biofuel cell. Electrochem Commun 9(2):331–336

25. Bedekar AS et al (2007) Oxygen limitation in microfluidic biofuel cells. Chem Eng Commun 195(3):256–266
26. Nazaruk E et al (2008) Enzymatic biofuel cell based on electrodes modified with lipid liquid-crystalline cubic phases. J Power Sources 183(2):533–538
27. Tamaki T, Yamaguchi T (2006) High-surface-area three-dimensional biofuel cell electrode using redox-polymer-grafted carbon. Ind Eng Chem Res 45(9):3050–3058
28. Matsue T et al (1985) Electron-transfer reactions associated with host-guest complexation. Oxidation of ferrocenecarboxylic acid in the presence of .beta.-cyclodextrin. J Am Chem Soc 107(12):3411–3417
29. Yan Y-M, Yehezkeli O, Willner I (2007) Integrated, electrically contacted NAD(P)+−dependent enzyme–carbon nanotube electrodes for biosensors and biofuel cell applications. Chem Eur J 13(36):10168–10175
30. Li X et al (2008) A miniature glucose/O2 biofuel cell with single-walled carbon nanotubes-modified carbon fiber microelectrodes as the substrate. Electrochem Commun 10(6):851–854
31. Gao F et al (2007) An enzymatic glucose/O2 biofuel cell: preparation, characterization and performance in serum. Electrochem Commun 9(5):989–996
32. Yan Y et al (2006) Carbon-nanotube-based glucose/O2 biofuel cells. Adv Mater 18 (19):2639–2643
33. Vidaković-Koch T et al (2013) Application of electrochemical impedance spectroscopy for studying of enzyme kinetics. Electrochim Acta 110:94–104
34. Vidaković-Koch TR et al (2011) Nonlinear frequency response analysis of the Ferrocyanide oxidation kinetics. Part I. A theoretical analysis. J Phys Chem C 115(35):17341–17351
35. Do TQN et al (2015) Dynamic and steady state 1-D model of mediated electron transfer in a porous enzymatic electrode. Bioelectrochemistry 106(Part A):3–13
36. Vidaković-Koch T et al (2017) Catalyst layer modeling. In: Breitkopf C, Swider-Lyons K (eds) Springer handbook of electrochemical energy. Springer Berlin Heidelberg, Berlin, pp 259–285
37. Bard A, Faulkner L (2001) Electrochemical methods, fundamentals and applications. Wiley, New York
38. Bartlett PN (2008) In: Bartlett PN (ed) Bioelectrochemistry: fundamentals, experimental techniques and applications. Wiley, New York
39. Varnicic M et al (2014) Combined electrochemical and microscopic study of porous enzymatic electrodes with direct electron transfer mechanism. RSC Adv 4(69):36471–36479
40. Varničić M, Vidaković-Koch T, Sundmacher K (2015) Gluconic acid synthesis in an electroenzymatic reactor. Electrochim Acta 174:480–487
41. Varničić M, Vidaković-Koch T, Sundmacher K (2015) Corrigendum to "Gluconic acid synthesis in an Electroenzymatic reactor" [Electrochimica Acta 174 (2015) 480–487]. Electrochim Acta 176:1523
42. Ivanov I (2012) Development of a glucose-oxygen enzymatic fuel cell. Otto von Guericke University, Magdeburg, p 118
43. Ivanov I, Vidaković-Koch T, Sundmacher K (2013) Alternating electron transfer mechanism in the case of high-performance tetrathiafulvalene–tetracyanoquinodimethane enzymatic electrodes. J Electroanal Chem 690:68–73
44. Vidakovic-Koch T (2017) Energy conversion based on bio(electro)catalysts. In: Cornelia Breitkopf KS-L (ed) Springer handbook of electrochemical energy. Springer-Verlag Berlin Heidelberg, Berlin, pp 757–777
45. Mondal MS, Fuller HA, Armstrong FA (1996) Direct measurement of the reduction potential of catalytically active cytochrome c peroxidase compound I: voltammetric detection of a reversible, cooperative two-electron transfer reaction. J Am Chem Soc 118(1):263–264
46. Mondal MS, Goodin DB, Armstrong FA (1998) Simultaneous voltammetric comparisons of reduction potentials, reactivities, and stabilities of the high-potential catalytic states of wild-type and distal-pocket mutant (W51F) yeast cytochrome c peroxidase. J Am Chem Soc 120 (25):6270–6276

47. Ruzgas T et al (1995) Kinetic models of horseradish peroxidase action on a graphite electrode. J Electroanal Chem 391(1):41–49
48. Ferapontova EE, Gorton L (2001) Effect of proton donors on direct electron transfer in the system gold electrode–horseradish peroxidase. Electrochem Commun 3(12):767–774
49. Yu H et al (2015) Influence of the ionomer/carbon ratio for low-Pt loading catalyst layer prepared by reactive spray deposition technology. J Power Sources 283:84–94
50. Lojou É, Bianco P (2004) Membrane electrodes for protein and enzyme electrochemistry. Electroanalysis 16(13–14):1113–1121
51. De Poulpiquet A et al (2013) Exploring properties of a hyperthermophilic membrane-bound hydrogenase at carbon nanotube modified electrodes for a powerful H2/O2 biofuel cell. Electroanalysis 25(3):685–695
52. Lojou É et al (2008) Biocatalysts for fuel cells: efficient hydrogenase orientation for H2 oxidation at electrodes modified with carbon nanotubes. JBIC, J Biol Inorg Chem 13 (7):1157–1167
53. Luo X et al (2009) Immobilization of the hyperthermophilic hydrogenase from Aquifex aeolicus bacterium onto gold and carbon nanotube electrodes for efficient H2 oxidation. JBIC, J Biol Inorg Chem 14(8):1275–1288
54. Lojou E (2011) Hydrogenases as catalysts for fuel cells: strategies for efficient immobilization at electrode interfaces. Electrochim Acta 56(28):10385–10397
55. Yan Y, Su L, Mao L (2007) Multi-walled carbon nanotube-based glucose/O2 biofuel cell with glucose oxidase and Laccase as biocatalysts. J Nanosci Nanotechnol 7(4–1):1625–1630
56. Khan GF (1997) TTF-TCNQ complex based printed biosensor for long-term operation. Electroanalysis 9(4):325–329
57. Khan GF (1996) Construction of SEC/CTC electrodes for direct electron transferring biosensors. Sens Actuators B Chem 36(1–3):484–490
58. Khan GF, Ohwa M, Wernet W (1996) Design of a stable charge transfer complex electrode for a third-generation amperometric glucose sensor. Anal Chem 68(17):2939–2945
59. Ivanov I, Vidaković-Koch T, Sundmacher K (2011) Direct hybrid glucose–oxygen enzymatic fuel cell based on tetrathiafulvalene–tetracyanoquinodimethane charge transfer complex as anodic mediator. J Power Sources 196(22):9260–9269
60. Do TQN (2017) Mathematical modelling of electro-enzymatic system. Otto von Guericke University, Magdeburg
61. Kochius S et al (2014) Electrochemical regeneration of oxidised nicotinamide cofactors in a scalable reactor. J Mol Catal B Enzym 103:94–99
62. Gorton L, Domínguez E (2007) Electrochemistry of NAD(P)+/NAD(P)H. Encyclopedia of electrochemistry. Wiley-VCH Verlag GmbH & Co. KGaA, Weinheim
63. Karyakin AA, Ivanova YN, Karyakina EE (2003) Equilibrium (NAD+/NADH) potential on poly(neutral red) modified electrode. Electrochem Commun 5(8):677–680
64. Arechederra MN, Addo PK, Minteer SD (2011) Poly(neutral red) as a NAD+ reduction catalyst and a NADH oxidation catalyst: towards the development of a rechargeable biobattery. Electrochim Acta 56(3):1585–1590
65. Karyakin AA et al (1999) Electropolymerized azines: part II. In a search of the best electrocatalyst of NADH oxidation. Electroanalysis 11(8):553–557
66. Li H, Wen H, Calabrese Barton S (2012) NADH oxidation catalyzed by electropolymerized azines on carbon nanotube modified electrodes. Electroanalysis 24(2):398–406
67. Rincón RA et al (2011) Flow-through 3D biofuel cell anode for NAD+−dependent enzymes. Electrochim Acta 56(5):2503–2509
68. Vuorilehto K, Lütz S, Wandrey C (2004) Indirect electrochemical reduction of nicotinamide coenzymes. Bioelectrochemistry 65(1):1–7
69. Salimi A et al (2009) Electrocatalytic reduction of NAD+ at glassy carbon electrode modified with single-walled carbon nanotubes and Ru(III) complexes. J Solid State Electrochem 13 (3):485–496

70. Ali I, Soomro B, Omanovic S (2011) Electrochemical regeneration of NADH on a glassy carbon electrode surface: the influence of electrolysis potential. Electrochem Commun 13 (6):562–565
71. Tosstorff A et al (2014) Mediated electron transfer with monooxygenases—insight in interactions between reduced mediators and the co-substrate oxygen. J Mol Catal B Enzym 108:51–58
72. Tosstorff A et al (2017) Towards electroenzymatic processes involving old yellow enzymes and mediated cofactor regeneration. Eng Life Sci 17(1):71–76
73. Çekiç SZ et al (2010) Mediated electron transfer with P450cin. Electrochem Commun 12 (11):1547–1550
74. Ströhle FW et al (2013) A computational protocol to predict suitable redox mediators for substitution of NAD(P)H in P450 monooxygenases. J Mol Catal B Enzym 88:47–51